Supplementary information

S. Marbach, J. A. Zheng, M. Holmes-Cerfon

Contents

1 N-legged, one dimensional, caterpillar model

Note that unless specifically mentioned, in the entire supplementary information l is used as a shortcut notation for spring length relative to its rest length $l - l_0$.

1.1 Agreement of simulation and analytical results regardless of the value of ϵ for the 1-legged caterpillar

In Fig. S1 we present agreement between the effective diffusion evaluated using stochastic simulations and evaluated with the analytical formula Eq. (12) of the main paper.

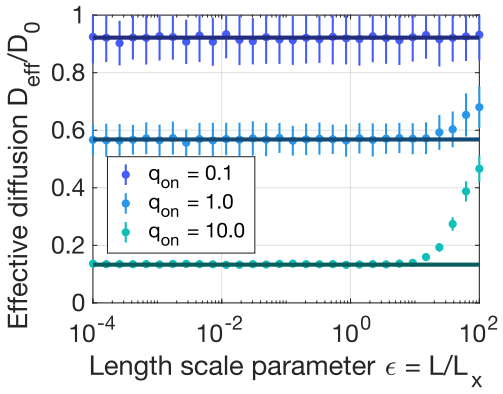

Figure S1: Simulation results for different values of the non-dimensionalizing parameter $\epsilon = L/L_x$ characterizing the difference between the length scale of oscillations of legs L versus the length scale of particle displacement L_x, for the case of a 1-legged caterpillar. Various values of the attachment rate q_{on} are explored (given in non-dimensional units $k/\Gamma\epsilon^2$). The other numerical parameters are $\gamma/\Gamma = 0.1$ and $q_{\text{off}} = 0.8k/\Gamma\epsilon^2$. The lines correspond to the analytical formula Eq. (12) of the main paper.

1.2 N legs facing a uniformly sticky surface

1.2.1 Method on an example: 2 legs facing a sticky surface

To investigate dynamics of caterpillars with multiple legs, we start by illustrating the framework on a 2 leg system.

Projection of the dynamics in the bound state The first step is to write the projected dynamics in the bound state. If there are 2 legs, when only 1 of them is bound, then the dynamics of the unbound leg are completely independent of the bound one and the projected bound equations are the same as those reported in the main paper. When 2 legs are bound however we must project again the dynamics. We therefore have 2 constraints $q_1(x, l_1, l_2) = x + l_1 + x_{r,1} = 0$ and $q_2(x, l_1, l_2) = x + l_2 + x_{r,2} = 0$ where x_r are reference positions when either of the legs first form their bond. The constraint matrix is therefore

$$C = (\nabla q)^T = \begin{pmatrix} 1 & 1 & 0 \\ 1 & 0 & 1 \end{pmatrix}. \tag{S1.1}$$

We then get the projector

$$P = I - C^T(CC^T)^{-1}C = \frac{1}{3}\begin{pmatrix} 1 & -1 & -1 \\ -1 & 1 & 1 \\ -1 & 1 & 1 \end{pmatrix} \tag{S1.2}$$

The friction matrix is in the unbound configuration

$$\tilde{\Gamma} = \begin{pmatrix} \Gamma & 0 & 0 \\ 0 & \gamma & 0 \\ 0 & 0 & \gamma \end{pmatrix} \tag{S1.3}$$

giving a projected friction and its Moore-Penrose pseudo-inverse as

$$\Gamma_P = P\tilde{\Gamma}P \quad = \tfrac{\Gamma+2\gamma}{3}P, \tag{S1.4}$$

$$\Gamma_P^\dagger \quad = \tfrac{1}{\Gamma+2\gamma}3P \tag{S1.5}$$

with a square root

$$\sigma_P = \sqrt{\Gamma_P^\dagger} = \frac{1}{\sqrt{\Gamma+2\gamma}} \begin{pmatrix} 1 & 0 & 0 \\ -1 & 0 & 0 \\ -1 & 0 & 0 \end{pmatrix}. \tag{S1.6}$$

We obtain the projected dynamics

$$\frac{dx}{dt} = -\frac{dl_1}{dt} = -\frac{dl_2}{dt} = \frac{k(l_1+l_2)}{\Gamma+2\gamma} + \sqrt{\frac{2k_BT}{\Gamma+2\gamma}}\eta(t) \tag{S1.7}$$

where $\eta(t)$ is a white Gaussian noise. The friction in the bound state is therefore naturally the sum of the frictions $\Gamma + 2\gamma$.

Generator for the dynamics For 2 legs we can write the full generator (in non-dimensional scales) $\mathcal{L}^{(2)} = \frac{1}{\epsilon^2}\mathcal{L}_0^{(2)} + \frac{1}{\epsilon}\mathcal{L}_1^{(2)} + \mathcal{L}_2^{(2)}$. The generator is now an operator acting on a space of 4 states (#1 has no bond, $\#2-3$ have 1 bond, where the leg 1 is bound in state #2 and reciprocally, and #4 has 2 bonds). The lowest order generator is

$$\mathcal{L}_0^{(2)} = \mathcal{Q}+\mathcal{U}_0 = \begin{pmatrix} -2q_{\text{on}} & q_{\text{on}} & q_{\text{on}} & 0 \\ q_{\text{off}} & -q_{\text{off}}-q_{\text{on}} & 0 & q_{\text{on}} \\ q_{\text{off}} & 0 & -q_{\text{off}}-q_{\text{on}} & q_{\text{on}} \\ 0 & q_{\text{off}} & q_{\text{off}} & 2q_{\text{off}} \end{pmatrix} + \text{diag} \begin{pmatrix} \frac{\Gamma}{\gamma}\left(D_{l_1}+D_{l_2}\right) \\ \frac{\Gamma}{\Gamma+\gamma}D_{l_1} + \frac{\Gamma}{\gamma}D_{l_2} \\ \frac{\Gamma}{\gamma}D_{l_1} + \frac{\Gamma}{\Gamma+\gamma}D_{l_2} \\ \frac{\Gamma}{\Gamma+2\gamma}\left(-(l_1+l_2)(\partial_{l_1}+\partial_{l_2}) + (\partial_{l_1}+\partial_{l_2})^2\right) \end{pmatrix} \tag{S1.8}$$

where $D_{l_i} = -l_i\partial_{l_i} + \partial_{l_i l_i}$ is an operator for the unbound tether i. The next orders are

$$\mathcal{L}_1^{(2)} = \text{diag} \begin{pmatrix} 0 \\ \frac{\Gamma}{\Gamma+\gamma}(l_1\partial_x - 2\partial_{xl_1}) \\ \frac{\Gamma}{\Gamma+\gamma}(l_2\partial_x - 2\partial_{xl_2}) \\ \frac{\Gamma}{\Gamma+2\gamma}((l_1+l_2)\partial_x - 2\partial_{xl_1} - 2\partial_{xl_2}) \end{pmatrix} \text{ and } \mathcal{L}_2^{(2)} = \text{diag} \begin{pmatrix} \partial_{xx} \\ \frac{\Gamma}{\Gamma+\gamma}\partial_{xx} \\ \frac{\Gamma}{\Gamma+\gamma}\partial_{xx} \\ \frac{\Gamma}{\Gamma+2\gamma}\partial_{xx} \end{pmatrix}. \tag{S1.9}$$

The equilibrium distribution is simply

$$\pi \propto \begin{pmatrix} (q_{\text{off}}/q_{\text{on}})^2 \\ q_{\text{off}}/q_{\text{on}} \\ q_{\text{off}}/q_{\text{on}} \\ 1 \end{pmatrix} e^{-l_1^2/2} e^{-l_2^2/2}. \tag{S1.10}$$

Long time solution We now seek a solution as an expansion in ϵ, $f = f_0 + \epsilon f_1 + ...$ In a very similar way as systematically observed in similar derivations we find $f_0 = a(x,t)\begin{pmatrix}1 & 1 & 1 & 1\end{pmatrix}^T$ at lowest order. The associated equilibrium distribution is $\pi_0 = \pi$. At the following order we need to solve $\mathcal{L}_0^{(2)} f_1 = -\mathcal{L}_1^{(2)} f_0$ and we will seek a natural solution (that strongly reflects the symmetry of the problem) as

$$f_1 = \begin{pmatrix} u_0 l_1 + u_0 l_2 \\ b_1 l_1 + u_1 l_2 \\ u_1 l_1 + b_1 l_2 \\ b_2 l_1 + b_2 l_2 \end{pmatrix} \partial_x a \tag{S1.11}$$

where u_n and b_n are constants that solve a linear system of equations (with non zero determinant), and u_n and b_n refer respectively to unbound and bound contributions with n bonds in the system. We do not report the equation system here but will come to it later on. At the next order, to find a solution for f_2 we require the Fredholm alternative, $\langle \partial_t f_0 - \mathcal{L}_2^{(2)} f_0 - \mathcal{L}_1^{(2)} f_1, \pi_0 \rangle = 0$, which gives

$$\left(\frac{q_{\text{off}}^2}{q_{\text{on}}^2} + \frac{2q_{\text{off}}}{q_{\text{on}}} + 1\right)\partial_t a = \frac{q_{\text{off}}^2}{q_{\text{on}}^2}\partial_{xx} a + 2\frac{q_{\text{off}}}{q_{\text{on}}}\frac{\Gamma}{\Gamma+\gamma}(1-b_1)\,\partial_{xx} a + (1-2b_2)\,\partial_{xx} a \tag{S1.12}$$

which can be rewritten as a weighted sum (in dimensional scales)

$$\partial_t a = k_B T \left(\frac{p_0}{\Gamma} + \frac{p_1}{\frac{\Gamma+\gamma}{(1-b_1)}} + \frac{p_2}{\frac{\Gamma+2\gamma}{(1-2b_2)}}\right)\partial_{xx} a \tag{S1.13}$$

where p_k is the probability to have k bonds ($p_0 = q_{\text{off}}^2/Z$, $p_1 = 2q_{\text{off}}q_{\text{on}}/Z$ and $p_2 = q_{\text{on}}^2/Z$ with $p_0 + p_1 + p_2 = 1$). The above expression clearly shows that the effective inverse friction is a weighted sum of inverse friction coefficients

$$\frac{1}{\Gamma_{\text{eff}}^{2\,\text{legs}}} = \sum_{n=0}^{2}\frac{p_n}{\Gamma_n} = \sum_{n=0}^{2}\frac{p_n}{\frac{\Gamma+n\gamma}{(1-nb_n)}}. \tag{S1.14}$$

We will show this expression for all N below. The linear system of equations solved by the u_k and b_k can now be given

$$\begin{aligned}
-2q_{\text{on}}u_0 + q_{\text{on}}b_1 + q_{\text{on}}u_1 - \frac{\Gamma}{\gamma}u_0 &= 0, \text{ (unbound contributions in the 0 bond state)} \\
q_{\text{off}}u_0 - q_{\text{off}}u_1 - q_{\text{on}}u_1 + q_{\text{on}}b_2 - \frac{\Gamma}{\gamma}u_1 &= 0, \text{ (unbound contributions in a 1 bond state)} \\
q_{\text{off}}u_0 - q_{\text{off}}b_1 - q_{\text{on}}b_1 + q_{\text{on}}b_2 - \frac{\Gamma}{\Gamma+\gamma}b_1 &= -\frac{\Gamma}{\Gamma+\gamma}, \text{ (bound contributions in a 1 bond state)} \\
q_{\text{off}}b_1 + q_{\text{off}}u_1 - 2q_{\text{off}}b_2 - 2\frac{\Gamma}{\Gamma+2\gamma}b_2 &= -\frac{\Gamma}{\Gamma+2\gamma}, \text{ (bound contributions in the 2 bonds state).}
\end{aligned} \tag{S1.15}$$

Solving the above linear system yields lengthy expressions for b_k and u_k. One can show however that the effective contributions for the bound states can be expanded as

$$\Gamma_1 = \Gamma + \gamma_{\text{eff}}\left(1 - O(\frac{\gamma_{\text{eff}}}{\Gamma})\right)\ \Gamma_2 = \Gamma + 2\gamma_{\text{eff}}\left(1 + O(\frac{\gamma_{\text{eff}}}{\Gamma})\right) \tag{S1.16}$$

such that we find already some a linear scaling as $\Gamma_n \sim \Gamma + n\gamma_{\text{eff}}$.

1.2.2 N legs

Projection of the dynamics with N legs. The projection formalism naturally extends to N legs. For n bound legs we find that the friction is simply $\Gamma + n\gamma$, such that the projected dynamics are for the first n bound legs

$$\frac{dx}{dt} = -\frac{dl_1}{dt} = ... = -\frac{dl_n}{dt} = \frac{k\sum_{i=1}^{n}(l_i)}{\Gamma + n\gamma} + \sqrt{2\frac{k_B T}{\Gamma + n\gamma}}\eta(t). \tag{S1.17}$$

System of equations for N legs The generator is now an operator acting on 2^N states, and we order these states according to their number of bonds (0 bonds, all 1 bond states, all 2 bonds states, ...). For N legs we can write the full generator (in non-dimensional scales) $\mathcal{L}^{(N)} = \frac{1}{\epsilon^2}\mathcal{L}_0^{(N)} + \frac{1}{\epsilon}\mathcal{L}_1^{(N)} + \mathcal{L}_2^{(N)}$, where all $\mathcal{L}_i^{(N)}$ terms are very similar to the ones introduced for $N = 2$ and can be naturally generalized. Similarly the equilibrium distribution is naturally extended as

$$\pi = e^{-\sum_{i=1}^N l_i^2/2}\left((q_{\text{off}}/q_{\text{on}})^N \quad (q_{\text{off}}/q_{\text{on}})^{N-1} \quad (q_{\text{off}}/q_{\text{on}})^{N-1} \quad .... \quad (q_{\text{off}}/q_{\text{on}})^{N-2} \quad ... \quad 1\right)^T. \tag{S1.18}$$

Long time solution with N legs We now seek a solution as an expansion in ϵ, $f = f_0 + \epsilon f_1 + ...$ In a very similar way as systematically observed in similar derivations we find $f_0 = a(x,t)\left(1 \quad ... \quad 1\right)^T$ at lowest order. The associated equilibrium distribution is $\pi_0 = \pi$. At the following order we need to solve $\mathcal{L}_0^{(N)} f_1 = -\mathcal{L}_1^{(N)} f_0$ and we will seek a natural solution (that strongly reflects the symmetry of the problem) as

$$f_1 = \begin{pmatrix} u_0 l_1 + u_0 l_2 + ... + u_0 l_N \\ b_1 l_1 + u_1 l_2 + ... + u_1 l_N \\ u_1 l_1 + b_1 l_2 + ... + u_1 l_N \\ ... \\ b_2 l_1 + b_2 l_2 + u_2 l_3 ... + u_2 l_N \\ ... \\ b_N l_1 + b_N l_2 + ... + b_N l_N \end{pmatrix} \partial_x a \tag{S1.19}$$

where u_n and b_n refer respectively to unbound and bound contributions with n bonds in the system. We now seek the general system of equations satisfied by u_n and b_n. For a number of bonds n, consider that a given focus tether is unbound, say i. This will therefore allow us to obtain an equation on the unbound contributions of that tether (that in l_i) so primarily on u_n. The tether is relaxing yielding a contribution $-\frac{\Gamma}{\gamma}u_n$. There are n possible bonds to undo leading to a contribution $(-nq_{\text{off}}u_n)$. In any $n-1$ bond configurations starting from our initial configuration, the focus tether will still be unbound (u_{n-1}), such that we get an $(+nq_{\text{off}}u_{n-1})$ contribution. There are $N-n$ bonds to form $(-(N-n)q_{\text{on}}u_n)$. In forming bonds, only 1 choice yields to bind the focus tether $(q_{\text{on}}b_{n+1})$ while the other forming bonds will not be the focus tether $((N-n-1)q_{\text{on}}u_{n+1})$. The right hand side terms (from $\mathcal{L}_1^{(N)}f_0$) corresponding to unbound tethers are 0. This yields the first line of the system of equations Eq. (S1.20) below. If one considers a bound focus tether, similarly one can derive contributions due to binding and unbinding. The bound relaxation terms yield a contribution $(-\frac{n\Gamma}{\Gamma+n\gamma}b_n)$. Additionally, the right hand side terms (coming from $\mathcal{L}_1^{(N)}f_0$) corresponding to the unbound tether is $-\frac{\Gamma}{\Gamma+n\gamma}$. We obtain

$$\begin{cases} nq_{\text{off}}u_{n-1} - nq_{\text{off}}u_n - (N-n)q_{\text{on}}u_n + q_{\text{on}}b_{n+1} + (N-n-1)q_{\text{on}}u_{n+1} - \dfrac{\Gamma}{\gamma}u_n = 0 \\ q_{\text{off}}u_{n-1} + (n-1)q_{\text{off}}b_{n-1} - nq_{\text{off}}b_n - (N-n)q_{\text{on}}b_n + (N-n)q_{\text{on}}b_{n+1} - \dfrac{n\Gamma}{\Gamma+n\gamma}b_n = -\dfrac{\Gamma}{\Gamma+n\gamma}. \end{cases} \tag{S1.20}$$

The system Eq. (S1.20) applies for all $n = 0..N$, taking as boundary equations $u_N = 0$ and $b_0 = 0$. Unfortunately the system does not simplify further but its determinant is non zero, showing that a non trivial solution exists. We will study it further later but for now conclude on the long time solution. At the next order, to find a solution for f_2 we require the Fredholm alternative, $\langle \partial_t f_0 - \mathcal{L}_2^{(N)} f_0 - \mathcal{L}_1^{(N)} f_1, \pi_0 \rangle = 0$, which yields after some algebraic manipulations (back in dimensional scales)

$$\partial_t a = k_B T \left(\frac{p_0}{\Gamma} + \frac{p_1}{\frac{\Gamma+\gamma}{(1-b_1)}} + \frac{p_2}{\frac{\Gamma+2\gamma}{(1-2b_2)}} + ... + \frac{p_N}{\frac{\Gamma+N\gamma}{(1-Nb_N)}} \right) \partial_{xx} a \tag{S1.21}$$

where $p_n = \frac{\binom{N}{n} x^n (1-x)^{N-n}}{Z}$ with $x = q_{\text{on}}/q_{\text{off}}$ is the probability to have n bonds. Writing in full generality

$$\Gamma_n = \frac{\Gamma + n\gamma}{(1 - nb_n)} \tag{S1.22}$$

we indeed recover Eq. (15) of the main manuscript. We also see that the coefficients Γ_n indeed correspond to friction contributions in a state with n bonds as only n and b_n, that corresponds to the bound contributions, intervene.

Resolution when the system is dominated by the average number of bonds We can search for a closed (simpler) system for Eq. (S1.20) where the dominant terms will originate from the average number of bonds $N_b = \sum_{n=0}^{N} n p_n = N \frac{q_{\text{on}}}{q_{\text{on}}+q_{\text{off}}}$. We assume that, around this average number, terms do not change much (the derivatives are close to 0), meaning we can approximate $u_{N_b} \simeq u_{N_b-1} \simeq u_{N_b+1} \equiv \bar{u}$, and similarly for $b_{N_b} = \bar{b}$ leading to

$$\begin{cases} -q_{\text{on}}\bar{u} + q_{\text{on}}\bar{b} - \frac{\Gamma}{\gamma}\bar{u} = 0 \\ q_{\text{off}}\bar{u} - q_{\text{off}}\bar{b} - \frac{N_b\Gamma}{\Gamma+N_b\gamma}\bar{b} = -\frac{\Gamma}{\Gamma+N_b\gamma} \end{cases} \tag{S1.23}$$

Solving the system for $\bar{b}$ and $\bar{u}$ yields then the value of the friction coefficient for the average number of bonds (back in dimensional scales)

$$\Gamma_{N_b} = \frac{\Gamma + N_b\gamma}{1 - N_b\bar{b}} = \Gamma + N_b\left(\gamma + \frac{k}{q_{\text{off}}} + \gamma\frac{q_{\text{on}}}{q_{\text{off}}}\right) \tag{S1.24}$$

Eq. (S1.24) is reported as Eq. (16) in the main text. It shows excellent agreement with the exact (numerical) solution to the full system of Eqs. S1.20 at large total number of legs N (see Fig. S2).

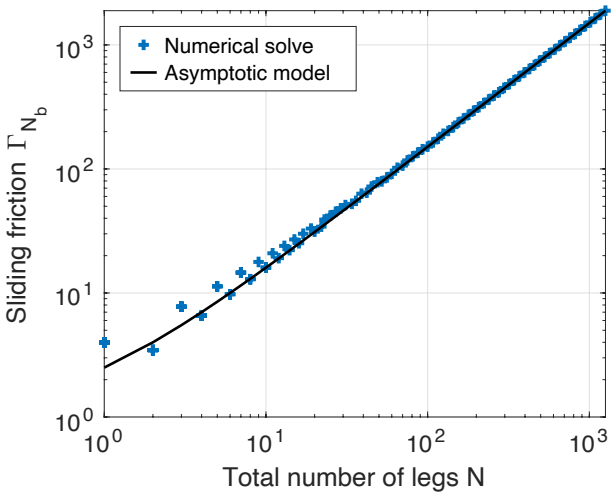

Figure S2: Value of friction coefficient for the average number of bonds as evaluated using Eq. (S1.24) or equivalently Eq. (15) of the main paper ("Asymptotic model") and fully solving the system of equations Eq. (S1.20) and presenting the value Γ_n for the index n closest to N_b ("Numerical solve"). Here the values of other parameters (in dimensional scales) are all set to $1 = \frac{q_{\text{on}}\Gamma}{k} = \frac{q_{\text{off}}\Gamma}{k} = \frac{\gamma}{\Gamma}$.

Empirical solution for an arbitrary number of bonds An interesting question is then to investigate Γ_n, the effective friction contributing to the state with n bonds, in the large N (total number of legs) limit. This requires solving the full system Eq. (S1.20). This system is not easily amenable to analytical calculations, and instead we use it as a benchmark to explore a phenomenological law for Γ_n.

First, it is natural to assume that the correction $\Gamma_n - \Gamma$ typically contains a term $n\gamma$ coming from added friction of the n bonds (as is noted already in the projected dynamics). Then, recall forces are also exerting

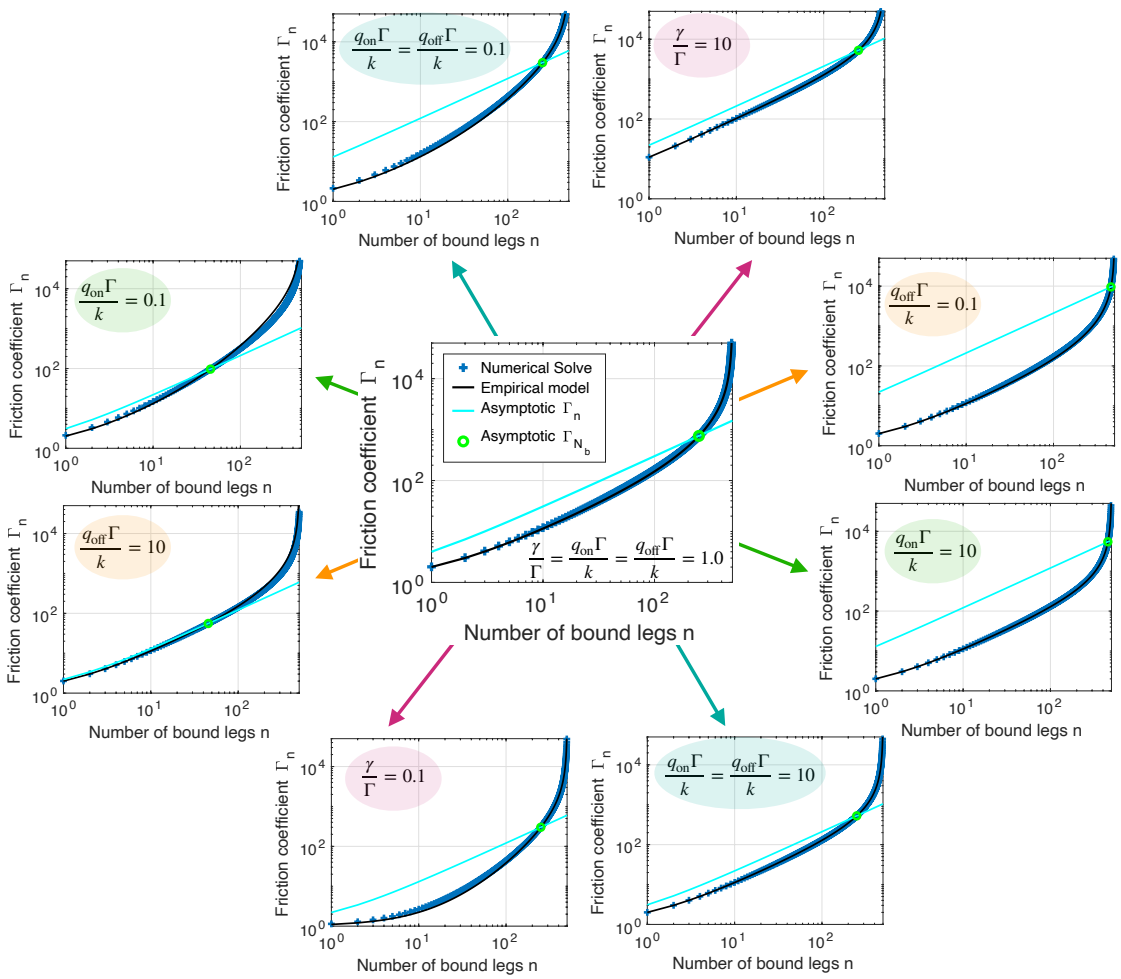

Figure S3: Value of friction coefficients Γ_n for all possible number of bonds (for a maximum of $N = 500$) as evaluated using Eq. (S1.27) ("Empirical model") and fully solving for the system of equations Eq. (S1.20) and presenting the values Γ_n ("Numerical Solve"). Index N_b is highlighted in green in each plot, and calculated from Eq. (16) . The "Asymptotic Γ_n" result corresponds to Eq. (S1.28). Here the values of other parameters (in dimensional scales) are all set to $1 = \frac{q_{on}\Gamma}{k} = \frac{q_{off}\Gamma}{k} = \frac{\gamma}{\Gamma}$ unless another indication is given.

friction. Typically n bonds are exerting friction due to recall forces. Yet for this final contribution to Γ_n, the situation is not the same for n bonds as for N_b bonds. Around $n = N_b$, the probabilities to be in a state with one more bond or one bond less are more or less the same, $p(N_b - 1) \simeq p(N_b) \simeq p(N_b + 1)$. For n bonds, we have in general (for example investigating the probability to undo a bond)

$$\begin{aligned}\frac{p(n)}{p(n-1)} &= \frac{\binom{N}{n} p_0^n (1-p_0)^{N-n}}{\binom{N}{n-1} p_0^{n-1} (1-p_0)^{N-n+1}} \\ &= \frac{\binom{N}{n} p_0^n (1-p_0)^{N-n} p_0}{\binom{N}{n} \frac{n}{N-n+1} p_0^n (1-p_0)^{N-n}(1-p_0)} \\ &= \frac{p_0}{(1-p_0)} \frac{N-n+1}{n} = \frac{N_b}{N-N_b} \frac{N-n+1}{n}\end{aligned} \tag{S1.25}$$

We expect that the typical time over which the spring resistance acts τ_{eff} has to be modified by the propensity

to unbind (coming from the state with n bonds) as $\tau_{\rm eff} \to \tau_{\rm eff}\frac{p(n-1)}{p(n)}$. We obtain, wrapping up all contributions

$$\Gamma_n = \Gamma + n\left(\gamma + k\tau_{\rm eff}\frac{p(n-1)}{p(n)}\right) = \Gamma + n\left(\gamma + k\frac{p(n-1)}{p(n)}\left[\frac{1}{q_{\rm off}} + \frac{\gamma}{k}\frac{q_{\rm on}}{q_{\rm off}}\right]\right). \tag{S1.26}$$

which explicitly writes as

$$\Gamma_n = \Gamma + n\left(\gamma + k\frac{N-N_b}{N-(n-1)}\frac{n}{N_b}\left[\frac{1}{q_{\rm off}} + \frac{\gamma}{k}\frac{q_{\rm on}}{q_{\rm off}}\right]\right) \tag{S1.27}$$

Eq. (S1.27) is compared to the full solution of the linear system in Fig. S3. We find excellent agreement over a broad range of parameters. Notice that also around $n \simeq N_b$ and for $N_b \ll N$ we find the limit behavior

$$\Gamma_n = \Gamma + n\left(\gamma + \left[\frac{k}{q_{\rm off}} + \gamma\frac{q_{\rm on}}{q_{\rm off}}\right]\right) \tag{S1.28}$$

which allows us to recover, as anticipated, the result for $n = N_b$ of Eq. (16) .

2 Comparison to experimental data for diffusion of DNA-coated colloids

2.1 Experimental data for the diffusion of DNA-coated colloids: I. Additional data

2.1.1 Preparation of material

DNA coated polystyrene colloids We synthesize DNA-coated polystyrene (PS) spheres using the swelling/deswelling method reported in Ref. [2]. Polystyrene-b-poly(ethylene oxide) copolymer PS(3800 g/mol)-b-PEO(6500 g/mol) is purchased from Polymer Source Inc, and is first functionalized with azide at the end of the PEO chain [3]. PS-b-PEO-N3 are then attached to the PS particles using the swelling/deswelling method. In the synthesis, 15 μL of 1μm particles (10 w/v, purchased from Thermo Scientific), 125 μL Deionized (DI) water, 160 μL tetrahydrofuran (THF) and 100 μL of PS-b-PEO-N3 are mixed at room temperature. The mixture is placed on a horizontal shaker (1000 rpm) for 1.5 hours to fully swell the PS particles and absorb the PS block of the PS-b-PEO-N3 molecules. Then THF is slowly removed from the solution via evaporation by adding DI water, leaving the hydrophobic PS blocks physically inserted into the particles and the hydrophilic PEO chains extending out into the solution. The particles are washed with DI water three times to remove excess polymers.

Single stranded DNA (ssDNA, 20 bases, purchased from Integrated DNA Technologies) with 5' dibenzocyclooctyne (DBCO) end modification, is clicked to the N3 (at the end of PS-b-PEO-N3) through strain promoted alkyne-azide cycloaddition [2]. PS particles previously coated with the PS-b-PEO-N3 polymer brush are dispersed in 200 μL of 500 mM PBS buffer, at pH 7.4. Then 10 μL of DBCO-DNA (0.1 mM) are added to the suspension. The mixture is left to react for 48 hours on a horizontal shaker (1000 rpm). The final product is washed in DI water three times and stored in 140 mM PBS buffer. The DNA coverage density is measured using flow cytometry and we obtain $\sigma = 1/(3.27\ \text{nm}^2)$. The DNA sequence used on the colloids is 5'-/DBCO/-T_{14}-ACCGCA-3'.

DNA coated glass substrate DNA coated substrates are prepared using the same swelling/deswelling method. First, an ultra thin PS layer is spin-coated to a cleaned 22 mm x 22 mm glass coverslip (purchased from Bioscience Tools). The substrate is then swelled in the same PS-b-PEO-N3 solution in THF for 4 hours. Then THF is slowly removed from the solution via evaporation. DNA clicking is performed in a home made PDMS reaction chamber for 48 hours on a shaking stage, then washed 10 times in DI water to remove extra DNA. The entire sample is sealed in the 140 mM PBS buffer (ph 7.4) with 0.3% w/v pluronic F127 surfactants, using UV glue to avoid any external flow or evaporation of the buffer. The DNA sequence used on the glass substrate is complementary to that on the particles, 5'-/DBCO/-T_{14}-TGCGGT-3'.

2.1.2 Tracking DNA coated colloids

Particle positions measurements To study the diffusion of DNA coated colloids, we track the motion of about 500 particles as they bind and diffuse on the DNA coated substrate – see Fig. S4-A. The sample is mounted on a homemade lab microscope (Nikon Eclipse Ti 60X, 72nm pixel size, depth of focus 560 nm) thermal stage with a temperature controller. Tracer particles fixed on the substrate are used to substract camera drift during the tracking. Displacement measurements are performed by tracking particles over the temperature range 28-62 °C – see Fig. S4-B. At each temperature, particles are tracked over a time range of 20 min at a frame rate of 5 images per second. For the highest temperature reported here, $T = 59.1$ °C, particles diffuse faster and we only track them over 5 min, with 10 images per second. Images are then analyzed using the TrackPy software to obtain individual particle positions with time. Particles that do not move at all even at high temperatures are removed from the analysis. These particles are likely in a low density area where steric repulsion is not sufficient to screen van der Waals attraction, and therefore are "crashed" on the surface.

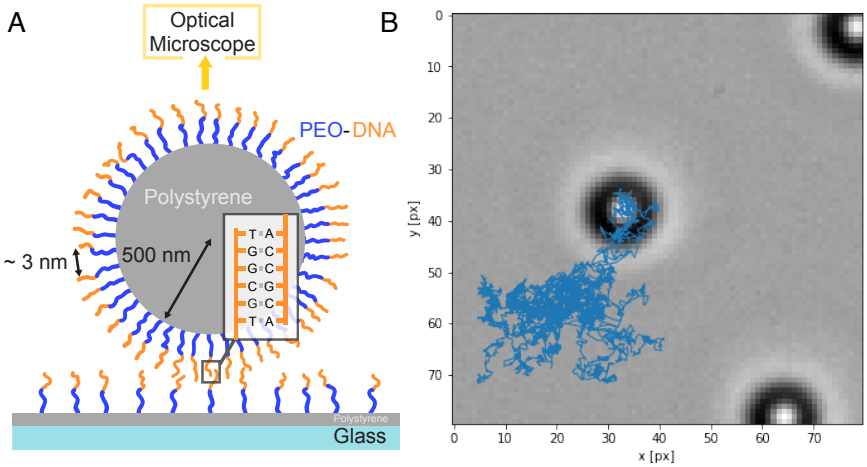

Figure S4: **Experimental setup to measure diffusion of DNA-coated colloids on DNA-coated surfaces.** (A) Schematic of a DNA-coated colloid attaching to a DNA-coated substrate, with the specific DNA sequence used in this study. Diffusion of the colloids is tracked from on-top. (B) Example of a colloid trajectory over an 18 min time frame (in blue) overlaid on the bright-field microscope image corresponding to the colloid's initial position. Here 1 px corresponds to 0.108 μm.

Mean square displacement analysis We fit the ensemble mean-squared displacement to a power law as $< \boldsymbol{x}^2(t) >= 4Dt^\alpha$, where $\boldsymbol{x}$ is the position of each particle on the surface plane, using a linear regression in log space to get the diffusion coefficient D and the power on time α. Typically, α decreases from ~ 1 at high temperatures to values < 1 at lower temperatures. Around the melting transition however, there exists a window of a few degrees where the motion is diffusive and we obtained $1.02 > \alpha > 0.94$. On this temperature window we then fix $\alpha = 1$ and the effective diffusivity D_{eff} is obtained by fitting the ensemble-averaged mean-square displacement to the power law $\langle \boldsymbol{x}^2(t) \rangle = 4D_{\text{eff}}t$.

Melting curve To compare different measurements with one another we define a kinetic melting temperature. This temperature T_m corresponds to the temperature for which the measured diffusion coefficient is half that of the high temperature diffusion coefficient (the latter corresponding to the hydrodynamic diffusion coefficient).

Reproducibility and error bars The entire experimental process (synthesis and mean square displacement measurements) are reproduced 3 times and the results are reported with different symbols in Fig. 7A of the main manuscript. Note that the synthesis is performed with slight variations of the coating process (shaking time), yet very similar behavior is obtained – for example the melting temperatures for each of

the samples are within 3°C of each other. Such disparity in melting temperature can occur due to density differences originating while performing the same synthesis and hence we do not report further details here.

As the average for D_{eff} is calculated over a great number of particles, the typical error on D_{eff}, for example due to the fitting procedure, is very small – typically smaller than the size of the points used to represent data and also much smaller than intrinsic disparities from sample to sample due to density fluctuations on the surface coverage during sample preparation. Therefore we do not report any vertical error bars. The exact temperature measured can slightly fluctuate, due to potential drift of the temperature controller, thus it is reasonable to assume a 0.2°C error bar on each experimental data point.

2.2 Experimental data for the diffusion of DNA-coated colloids: II. Existing data

Diffusion of DNA-coated colloids from existing data was obtained from 2 published references [4, 5].

High coating density diffusion coefficients from Ref. [5] Diffusion coefficients from Ref. [5] were obtained by fitting a linear law through extracted mean square displacement data using WebPlotDigitizer [6] – when the diffusion exponent α is greater than ~ 0.8. Mean square displacement data in Ref. [5] represents the projected mean square displacement $\langle \boldsymbol{r}^2 \rangle$ covered on a half-sphere, when the displacement on the half-sphere is observed from on-top. The actual surface covered $\langle \boldsymbol{x}^2 \rangle$ is therefore larger than that measured on the projected area, and we can write $\langle \boldsymbol{x}^2 \rangle = \mathcal{A} \langle \boldsymbol{r}^2 \rangle$ where $\mathcal{A}$ is an area correction number. If the particle covers the entire area typically $\mathcal{A} \simeq 2$ since $2\pi R^2$ is the actual area of the half sphere of radius R, and πR^2 is the projected area. This typically accounts for the fact that the particles does not spend the same amount of time on the sides of the half-sphere and on the top, and that on the sides displacements can be fully orthogonal to the observation projection plane. Additionally, since motion is constrained to the half-sphere, in practice the random walk is constrained and folded back onto the sphere. If it were unconstrained on the sphere we would typically have $4\pi R^2$ of area covered projected on πR^2 so we take $\mathcal{A} = 4$ as an upper bound on $\mathcal{A}$. $\mathcal{A} = 2$ is our lower bound. These bounds allow us to define error bars for the diffusion data of Ref. [5]. Again, considering potential density fluctuations on either surfaces and other experimental uncertainties due to calibration of the temperature controller, it is reasonable to assume a 0.2°C error bar on each experimental data point.

The detailed parameters of the DNA-coated colloids used in Ref. [5] are provided in that reference and we use their specific values to perform analytical predictions for D_{eff}, see details below. The melting temperature in Ref. [5] is defined as the temperature for which the fraction of single particles is 50%, since the particles can self-assemble in arrays. This is a typical thermodynamic quantity hence we use a the thermodynamic definition of melting [7]

$$p_{\text{unbound}}^{Ref.\ [5]} = 1 - \frac{1}{Z} \int_0^{h_c} e^{-\phi(h)/k_B T} dh \tag{S2.1}$$

where $\phi(h)$ is a particle-particle interaction potential, $h_c \simeq 20$ nm is a typical interaction range and Z a normalization constant. We find without any fitting that $T_m^{\text{theo}} = 25.3$°C which is not too far from the experimental melting temperature $T_m = 28.9$°C. The difference is likely due to the slightly different method used to quantify T_m. We align experimental data relative to T_m and theoretical data relative to T_m^{theo}.

Low coating density diffusion coefficients from Ref. [4] Ref. [4] provides the diffusion coefficients for their DNA-coated particles above the melting temperature $T_m = 44.7$°C as $D_{\text{eff}}(47^\circ\ \text{C}) = 0.38\ \mu\text{m}^2/\text{s}$, and at the melting temperature $D_{\text{eff}}(44.7^\circ\ \text{C}) = 1.4 \times 10^{-3}\ \mu\text{m}^2/\text{s}$. Additionally, for the data provided 0.27° C below T_m, the exponent for diffusion is $\alpha \sim 0.8$ and we can estimate the diffusion coefficient from a linear fit to the data. We obtain $D_{\text{eff}}(44.5^\circ\ \text{C}) = \frac{30\ \mu\text{m}^2}{30000\text{s} \times 4} = 0.25 \times 10^{-3}\ \mu\text{m}^2/\text{s}$.

The detailed parameters of the DNA-coated colloids used in Ref. [4] are provided in that reference and we use their respective values to perform analytical predictions for D_{eff}, see details below. The melting temperature in Ref. [4] is defined as the temperature for which the fraction of moving particles is 50%, where " Moving is defined as a displacement larger than 50 nm (1 pixel) between frames (frame rate = 1 Hz)". We

can relate to this moving quantity by defining the unbound probability as

$$p_{\text{unbound}}^{Ref.\ [4]} = 1 - \text{erf}\left(\frac{\Delta x_{\max}}{\sqrt{4D_{\text{eff}}\Delta t_{\max}}}\right) \tag{S2.2}$$

measuring the probability that a step is larger than $\Delta x_{\max} = 50$ nm during a time interval $\Delta t_{\max} = 1$ s where the diffusion coefficient of the particle is D_{eff}. Here we use D_{eff} as predicted by hopping motion only since only hopping is occurring in this sample due to geometrical constraints. We find $T_m^{\text{theo}} = 44.2°\text{C}$ close to the experimental measurement of $T_m = 44.7°\text{C}$. We align experimental data relative to T_m and theoretical data relative to T_m^{theo}. In line with previous analysis we also add 0.2°C error bar on each experimental data point.

2.3 Modeling tools for DNA-coated colloids

2.3.1 Number of legs and average number of bonds

To evaluate D_{eff} from Eq. (15) , we must evaluate the parameters of the 1D nanocaterpillar model. As mentioned in the main manuscript, some parameters, such as N and N_b (or equivalently N and the ratio $q_{\text{on}}/q_{\text{off}}$) require careful modeling of the detailed leg-arm interactions [7] to be estimated.

We thus calculate the detailed DNA-DNA brush interactions, accounting for leg density, leg length and DNA sequence, by evaluating the interaction energy $\phi(h)$ of the DNA-coated colloid with another coated surface at separation distance h. Following Ref. [7], $\phi(h)$ includes repulsive steric interactions [8] and attractive binding interactions, with entropic terms due to loss of degrees of freedom upon binding and competition for binding partners [9].

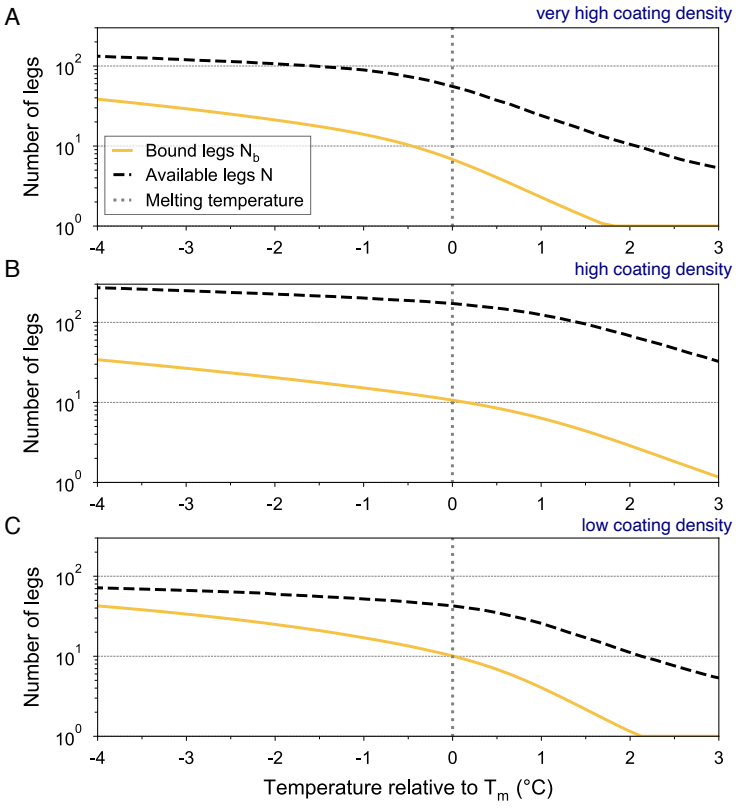

Figure S5: **Number of legs N and average number of bonds N_b involved in the binding process predicted from theory.** N and N_b are evaluated from detailed microscopic interactions for each system corresponding to detailed design parameters of DNA-coated colloids used (A) in this work (B) in Ref. [5] and (C) in Ref. [4].

All parameters are precisely known in the experimental system, but one: the coating density. We can estimate it by looking at the thermodynamic unbound probability obtained from the Boltzmann distribution as $p_u \sim \int_0^{h_c} e^{-\beta\phi(h)} dh$, and comparing it to the similar quantity calculated experimentally. The experimental data shows that the unbound probability transitions around $T_m = 55-58°$ C which corresponds to theoretical curves obtained with a surface density ranging from 1 DNA per $(9\text{ nm})^2$ to $(12\text{ nm})^2$. We therefore use 1 DNA per $(10.5\text{ nm})^2$ as a center value and the extremal values to calculate a fidelity interval for D_{eff} (gray area in Fig. 6A). These obtained values are within the range of expected values [7].

The average number of bonds N_b (gold in Fig. S5) and the number of legs within reach N (dashed black) with respect to temperature are then readily evaluated from the model leading to $\phi(h)$. The number of bonds at the melting temperature is only $N_b(T_m) \simeq 10$ while the number of available legs can be quite high $N(T_m) \simeq 100$. The number of bonds N_b increases strongly with decreasing temperature, from 0 to 40 over the 4°C window, thus potentially accounting for most of the decrease in diffusion.

2.3.2 3D geometry

In general the particle can explore positions not just in one dimension but in 3D. Here we discuss how to take into account this full geometry.

Second lateral dimension The second lateral dimension is – to some extent – a trivial extension of the 1-lateral dimension model derived in the main manuscript. We consider the constitutive equations for the leg and the particle in 2 lateral dimensions (x, y), simplifying here to $\ell_0 = 0$, namely considering that the rest state of the tether lies right above the surface and that deformations are still quadratic in the leg extension. We have

$$\frac{d\boldsymbol{l}}{dt} = -\frac{k}{\gamma}|\boldsymbol{l}|\frac{\boldsymbol{l}}{|\boldsymbol{l}|} + \sqrt{2\frac{k_BT}{\gamma}}\boldsymbol{\eta_l}$$
$$\frac{d\boldsymbol{x}}{dt} = +\sqrt{2\frac{k_BT}{\gamma}}\boldsymbol{\eta_x}.$$

The leg extension $\boldsymbol{l}$ is readily projected on both coordinates:

$$|\boldsymbol{l}|\frac{\boldsymbol{l}}{|\boldsymbol{l}|} = \boldsymbol{l} = l_x\boldsymbol{u}_x + l_y\boldsymbol{u}_y$$

and similarly for the noise operators. We obtain

$$\frac{dl_i}{dt} = -\frac{k}{\gamma}l_i + \sqrt{2\frac{k_BT}{\gamma}}\eta_{l,i}$$
$$\frac{dx_i}{dt} = +\sqrt{2\frac{k_BT}{\gamma}}\eta_{x,i}.$$

where $i = (x, y)$ refers to both lateral dimensions. The equations are fully uncoupled and hence it is not necessary to conduct further calculations to conclude that the effective long time motion should write as

$$\frac{d\boldsymbol{x}}{dt} = +\sqrt{2D_{\text{eff}}}\boldsymbol{\eta_x}.$$

where D_{eff} has the same expression as in the main manuscript.

Vertical dimension The particle may also venture far from the surface, where binding is not possible. To account for this 3D geometry, we use an extension of our main model.

One option to account for such a 2D dependence is to add a vertical degree of freedom say z for the particle, together with spatially dependent rates $q_{\text{on}}(z), q_{\text{off}}(z)$. This is not a trivial modification, especially as there are different ways to set the spatial dependence z of $q_{\text{on}}(z), q_{\text{off}}(z)$ (see for example the variability between Refs. [10, 11, 12]).

Instead we rely on a simplified geometrical approach, that has been shown to accurately reproduce a 2D geometry in another context [13], where we describe the system with 2 × 1D lines. For a 1-legged particle, we consider that the particle can switch between two regions where its dynamics are constrained to 1D:

surface and bulk regions. The particle enters the surface region with rate $Q_{\rm on}$, and then can bind to the surface with rate $q_{\rm on}$. If the particle is *unbound* in the surface region, it may lift off from the surface region to the bulk region with rate $Q_{\rm off}$. $\frac{Q_{\rm on}}{Q_{\rm off}}$ corresponds to the ratio of positions where the receptors are within and beyond reach. In DNA-coated colloid explorations, where particles are considered on top of a sticky surface, the ratio can be small or large depending on the density mismatch between the particle material and the surrounding fluid, that is otherwise described by the particle's gravitational height [4]. For other systems, such as white blood cells that are confined within blood vessels, particles are always close to the wall [14] and hence the ratio is quite large. Approach and lift-off from the surface are slow processes that scale like the diffusive dynamics of the particle and thus we may assume $Q_i\tau \sim O_\epsilon(1)$.

Performing similar coarse-graining steps (see following paragraph), we obtain an effective friction

$$\frac{1}{\Gamma_{\rm eff}^{2\times 1D}} = \frac{p_0^{2\times 1D}}{\Gamma_0} + \frac{p_1^{2\times 1D}}{\Gamma_1} \tag{S2.3}$$

where the probability to be in either states takes into account the added degree of freedom, $p_1^{2\times 1D} = Q_{\rm on}q_{\rm on}/Z$ and $p_0^{2\times 1D} = q_{\rm off}(Q_{\rm on}+Q_{\rm off})/Z$ with Z a normalization constant such that $p_0^{2\times 1D} + p_1^{2\times 1D} = 1$. The added degree of freedom does not change the result of Eq. (12) , simply the mathematical interpretation of the probability factors. Note that this framework has been verified against numerical simulations.

The values of $Q_{\rm on}$ and $Q_{\rm off}$ can be evaluated from the detailed interaction potential $\phi(h)$ of a DNA-coated colloid and the surface. In fact, the probability to be near the surface, in the absence of binding, is measured by

$$\frac{Q_{\rm on}}{Q_{\rm on}+Q_{\rm off}} = \int_0^{h_p} e^{-\beta(\phi(h)-\phi_{\rm bind}(h))}dh/Z \tag{S2.4}$$

where $\phi_{\rm bind}(h)$ measures the contributions to the interaction potential due to binding, $h_p \simeq 20$ nm measures the typical width of attractive interactions (region of space where binding could happen) and Z is a normalizing factor. For our DNA-coated colloids we find $\frac{Q_{\rm on}}{Q_{\rm on}+Q_{\rm off}} \simeq 0.0015$ and that the ratio does not depend much on temperature. It also does not depend significantly on the exact value of h_p for $h_p = 2-40$ nm.

For an N-legged caterpillar, the result generalizes to a change in the probability factors p_n in Eq. (15) for $D_{\rm eff}$. We have $p_0^{2\times 1D} = q_{\rm off}^N(Q_{\rm on}+Q_{\rm off})/Z$ and $p_n^{2\times 1D} = \binom{N}{n} q_{\rm off}^{N-n} q_{\rm on}^n Q_{\rm on}/Z$ such that $Z = Q_{\rm on}(q_{\rm on}+q_{\rm off})^N + Q_{\rm off}q_{\rm off}^N$.

2.3.3 2×1D, 1 legged nanocaterpillar model

In this section we derive the effective 1-legged long term caterpillar dynamics in an effective "2D" geometry by using the 2×1D mapping. The steps are carefully detailed so as to serve as an additional pedagogical explanation of the coarse-graining procedure introduced in the main text.

Constitutive equations of the 2×1D, 1-legged caterpillar model Let $p(x,l,t) = (p_V, p_u, p_b)^T$ be the probability distribution function of finding the system at time t in state x, l far from the surface (V), or close to the surface with a bound (b) or an unbound (u) leg. It obeys the Schmoluchowski equation

$$\partial_t p = \mathcal{L}^\star p \text{ with } \mathcal{L}^\star = \mathcal{Q}^\star + \mathcal{U}^\star \tag{S2.5}$$

where $\mathcal{Q}^\star$ is the matrix of rates to going from one state to another

$$\mathcal{Q}^\star = \begin{pmatrix} -Q_{\rm on} & Q_{\rm off} & 0 \\ Q_{\rm on} & -Q_{\rm off}-q_{\rm on} & q_{\rm off} \\ 0 & q_{\rm on} & -q_{\rm off} \end{pmatrix} \tag{S2.6}$$

and $\mathcal{U}^\star$ contains the dynamics in each state

$$\mathcal{U}^\star = \text{diag}\begin{pmatrix} \partial_l\left(\frac{k}{\gamma}(l-l_0) + \frac{k_BT}{\gamma}\partial_l\right) + \frac{k_BT}{\Gamma}\partial_{xx} \\ \partial_l\left(\frac{k}{\gamma}(l-l_0) + \frac{k_BT}{\gamma}\partial_l\right) + \frac{k_BT}{\Gamma}\partial_{xx} \\ (\partial_l-\partial_x)\left(\frac{k}{\Gamma+\gamma}(l-l_0) + \frac{k_BT}{\Gamma+\gamma}(\partial_l-\partial_x)\right) \end{pmatrix}. \tag{S2.7}$$

Consistently, the equilibrium distribution $\pi = \frac{e^{-\beta k(l-l_0)^2/2}}{Z}\left(\frac{Q^{\rm off}}{Q^{\rm on}}, \quad 1, \quad \frac{q_{\rm on}}{q_{\rm off}}\right)^T$ is indeed a stationary solution of Eq. (S2.5). Note that here $Q_{\rm on}$ and $Q_{\rm off}$ represent respectively the rates at which the particle approaches and leaves the vicinity of the surface, namely the region of space where binding is possible.

Non-dimensionalization Using the non-dimensional notation introduced in the main text allows to separate the Schmoluchowski operator $\mathcal{L}^\star$ in fast and slow operators. In the following, it will be somewhat easier to conduct the reasoning not on $\mathcal{L}^\star$ but on its adjoint $\mathcal{L}$, the generator of the system, defined such that for appropriate functions f, we have $\langle f, \mathcal{L}^\star p\rangle = \langle \mathcal{L} f, p\rangle$, where $\langle f, g\rangle = \iint (f_V g_V + f_u g_u + f_b g_b) dl dx$ is the inner product. We therefore seek a solution f of the dynamics

$$\partial_t f = \mathcal{L} f = \left(\frac{1}{\epsilon^2}\mathcal{L}_0 + \frac{1}{\epsilon}\mathcal{L}_1 + \mathcal{L}_2\right) \tag{S2.8}$$

where

$$\mathcal{L}_0 = \begin{pmatrix} \frac{\Gamma}{\gamma}(-l\partial_l + \partial_{ll}) & 0 & 0 \\ 0 & -q_{\rm on} + \frac{\Gamma}{\gamma}(-l\partial_l + \partial_{ll}) & q_{\rm on} \\ 0 & q_{\rm off} & -q_{\rm off} + \frac{\Gamma}{\Gamma+\gamma}(-l\partial_l + \partial_{ll}) \end{pmatrix}, \tag{S2.9}$$

$$\mathcal{L}_1 = \mathrm{diag}\left(0, 0, \frac{\Gamma}{\Gamma+\gamma}\left(l\partial_x - 2\partial_{lx}\right)\right) \tag{S2.10}$$

and

$$\mathcal{L}_2 = \begin{pmatrix} -Q_{\rm on} & Q_{\rm on} & 0 \\ Q_{\rm off} & -Q_{\rm off} & 0 \\ 0 & 0 & 0 \end{pmatrix} + \mathrm{diag}\left(1, 1, \frac{\Gamma}{\Gamma+\gamma}\right)\partial_{xx}. \tag{S2.11}$$

Additionally, f has to satisfy boundary conditions of no flux at infinity

$$\partial_l f(x, l, t)|_{l=\pm\infty} = 0 \tag{S2.12}$$

which correspond to the usual no flux in probability space (where the flux in probability space satisfies $(lp + \partial_l p)\,|_{l=\pm\infty} = 0$). This condition is physical as it imposes conservation of probability. Note that we expect these boundary conditions to be satisfied only at lowest order in ϵ.

Homogenization We seek a solution to Eq. (S2.8) as an expansion in the small parameter ϵ, as $f = f_0 + \epsilon f_1 + \epsilon f_2 + ...$ At lowest order we need to satisfy $\mathcal{L}_0 f_0 = 0$ which yields the general solution

$$f_0 = \begin{pmatrix} a_V(x,t) \\ a_S(x,t) \\ a_S(x,t) \end{pmatrix} + \int_0^l e^{y^2/2} dy \begin{pmatrix} b_V(x,t) \\ b_S(x,t) \\ b_S(x,t) \end{pmatrix} \tag{S2.13}$$

where a_S, a_V, b_S and b_V are all integration "constants" and S and V denote surface and volume terms. With the boundary conditions on f we get $b_S(x,t) = b_V(x,t) = 0$. Note that such boundary conditions also allow the cross product $\langle f_0, \pi\rangle$ to remain finite which will be expected later to use the Fredholm alternative.

The associated equilibrium distribution at lowest order π_0 spans a two dimensional space described by $(\pi_{0,V}(x,t), \pi_{0,S}(x,t))$ such that

$$\pi_0 = \frac{1}{Z}\begin{pmatrix} \pi_{0,V}(x,t) \\ \pi_{0,S}(x,t)) \\ \pi_{0,S}(x,t))\frac{q_{\rm on}}{q_{\rm off}} \end{pmatrix} e^{-l^2/2}. \tag{S2.14}$$

We therefore expect that our long time dynamics will consist in a 2×2 matrix describing the joint evolution of surface variables $(a_S(x,t))$ and volume variables $(a_V(x,t))$.

At the next order we need to satisfy $\mathcal{L}_0 f_1 = -\mathcal{L}_1 f_0$. f_1 is the sum of a particular integral and a complementary function (*i.e.* a function in the nullspace of $\mathcal{L}_0$). The complementary function can be taken to be 0 otherwise f_1 would contain terms that are redundant with f_0. One can check that the particular integral to this equation is simply

$$f_1 = \begin{pmatrix} 0 \\ \gamma q_{\text{on}} \\ \Gamma + \gamma q_{\text{on}} \end{pmatrix} \frac{l\partial_x a}{\Gamma(1+q_{\text{off}}) + \gamma(q_{\text{on}} + q_{\text{off}})}. \tag{S2.15}$$

At the following order we need to find a solution to $\mathcal{L}_0 f_2 = \partial_t f_0 - \mathcal{L}_2 f_0 - \mathcal{L}_1 f_1$. This equation has a solution if the right hand side terms of the equal sign satisfy the Fredholm alternative [15], namely

$$\langle \partial_t f_0 - \mathcal{L}_2 f_0 - \mathcal{L}_1 f_1, \pi_0 \rangle = 0. \tag{S2.16}$$

As π_0 spans a 2D space described by $(\pi_{0,V}(x,t), \pi_{0,S}(x,t))$ we can evaluate the Fredholm alternative on an orthogonal basis of this space; specifically here we will investigate the Fredholm alternative on $(1,0)$ then $(0,1)$. On the volume space we have

$$\partial_t a_V = \partial_{xx} a_V - Q_{\text{on}} a_V + Q_{\text{on}} a_S. \tag{S2.17}$$

On the surface space the terms are more lengthy and we split them for readability

$$\langle \partial_t f_0, \pi_0 \rangle = \left(1 + \frac{q_{\text{on}}}{q_{\text{off}}}\right) \partial_t a_S, \tag{S2.18}$$

$$\langle \mathcal{L}_2 f_0, \pi_0 \rangle = -Q_{\text{on}} a_S + Q_{\text{on}} a_V + \partial_{xx} a_S + \frac{q_{\text{on}}}{q_{\text{off}}} \partial_{xx} a \tag{S2.19}$$

and finally

$$\langle \mathcal{L}_1 f_1, \pi_0 \rangle = -\frac{q_{\text{on}}}{q_{\text{off}}} \frac{\Gamma + \gamma q_{\text{on}}}{\Gamma(1+q_{\text{off}}) + \gamma(q_{\text{on}} + q_{\text{off}})} \partial_{xx} a_S. \tag{S2.20}$$

Compiling all contributions on the surface we find

$$\begin{aligned} \partial_t a_S = &-Q_{\text{off}} a_S + Q_{\text{off}} a_V \\ &+ \frac{q_{\text{off}}}{q_{\text{off}} + q_{\text{on}}} \partial_{xx} a_S + \frac{q_{\text{off}}}{q_{\text{off}} + q_{\text{on}}} \frac{\Gamma}{\Gamma + \gamma \frac{1 + q_{\text{off}} + q_{\text{on}}}{q_{\text{off}}}} \partial_{xx} a_S. \end{aligned} \tag{S2.21}$$

Overall we have found effective long time dynamics described by the generator (in dimensional scales)

$$\mathcal{L}_{\text{eff}} = \begin{pmatrix} -Q_{\text{on}} + \frac{k_B T}{\Gamma} \partial_{xx} & Q_{\text{on}} \\ Q_{\text{off}} \frac{q_{\text{off}}}{q_{\text{on}} + q_{\text{off}}} & -Q_{\text{off}} \frac{q_{\text{off}}}{q_{\text{on}} + q_{\text{off}}} + \frac{k_B T}{\Gamma_{\text{eff}}} \partial_{xx} \end{pmatrix}, \text{ such that } \partial_t a = \mathcal{L}_{\text{eff}} a. \tag{S2.22}$$

Here $\Gamma_{\text{eff}}^{-1} = p_0 \Gamma_0^{-1} + p_1 \Gamma_1^{-1}$ with $\Gamma_0 = \Gamma$, $\Gamma_1 = \Gamma + \gamma + k\left(\frac{1}{q_{\text{off}}} + \frac{k}{\gamma} \frac{q_{\text{on}}}{q_{\text{off}}}\right)$, $p_0 = q_{\text{off}}/(q_{\text{off}} + q_{\text{on}})$ is the probability to have no bond near the surface and $p_1 = 1 - p_0$ is the probability to have 1 bond near the surface. Note that the expression of Γ_{eff} is exactly that when focusing only on surface dynamics and discarding effective 2D dynamics (see Eq. (12) of the main paper). This shows that homogenization steps in the embedded 2×1D geometry do not entangle with surface dynamics. To understand the meaning of this effective generator, we go one step further.

Long (long) times We now wish to understand the long time dynamics of the generator $\mathcal{L}_{\text{eff}}$. We search for long (long) time dynamics by using a non-dimensionalization that seeks even longer times as

$$t \to \tilde{t} \frac{\tau}{\epsilon}, \; x \to \tilde{x} L_x \tag{S2.23}$$

where $\tau = L_y^2/D_0 = L_y^2\Gamma/k_BT$ and $L_y/L_x = 1/\sqrt{\epsilon}$ corresponds to the far horizontal scales x is going to explore (compared to the shorter vertical scales). $Q_{\rm on}$ and $Q_{\rm off}$ are typically associated with the time scale that the particle takes to diffuse vertically and therefore $Q_{\rm on}\tau \sim 1$ and likewise $Q_{\rm off}\tau \sim 1$. We obtain the non-dimensional generator

$$\mathcal{L}_{\rm eff} = \frac{1}{\epsilon}\begin{pmatrix} -Q_{\rm on} & Q_{\rm on} \\ Q_{\rm off}\frac{q_{\rm off}}{q_{\rm on}+q_{\rm off}} & -Q_{\rm off}\frac{q_{\rm off}}{q_{\rm on}+q_{\rm off}} \end{pmatrix} + \begin{pmatrix} \partial_{xx} & 0 \\ 0 & \frac{\Gamma}{\Gamma_{\rm eff}}\partial_{xx} \end{pmatrix} = \frac{1}{\epsilon}\mathcal{L}_0 + \mathcal{L}_1 \tag{S2.24}$$

and we search for a solution f of the equation $\partial_t f = \mathcal{L}_{\rm eff} f$ expanded in ϵ as $f = f_0 + \epsilon f_1 + ...$

At lowest order we obtain from $\mathcal{L}_0 f_0 = 0$, $f_0 = a(x,t)\begin{pmatrix}1\\1\end{pmatrix}$, with the associated equilibrium distribution

$$\pi_0 = \frac{1}{Z}\begin{pmatrix} Q_{\rm off}\frac{q_{\rm off}}{q_{\rm on}+q_{\rm off}} \\ Q_{\rm on} \end{pmatrix}. \tag{S2.25}$$

At the next order we need to satisfy the Fredholm alternative, namely $\langle \partial_t f_0 - \mathcal{L}_1 f_0, \pi_0\rangle = 0$ leading to (back in dimensional scales)

$$\partial_t a = \frac{k_BT}{\Gamma_{\rm eff}^{2\times 1{\rm D}}}\partial_{xx} a \tag{S2.26}$$

where

$$\frac{1}{\Gamma_{\rm eff}^{2\times 1{\rm D}}} = \frac{Q_{\rm off}q_{\rm off}}{Q_{\rm off}q_{\rm off} + Q_{\rm on}\left(q_{\rm on}+q_{\rm off}\right)}\frac{1}{\Gamma} + \frac{Q_{\rm on}\left(q_{\rm on}+q_{\rm off}\right)}{Q_{\rm off}q_{\rm off} + Q_{\rm on}\left(q_{\rm on}+q_{\rm off}\right)}\frac{1}{\Gamma_{\rm eff}}. \tag{S2.27}$$

Expanding terms with the expression of $\Gamma_{\rm eff}$ and rearranging we can summarize the result in the explicit form, similarly as in Eq. (12) of the main paper,

$$\boxed{\frac{1}{\Gamma_{\rm eff}^{2\times 1{\rm D}}} = \frac{p_0^{2\times 1D}}{\Gamma_0} + \frac{p_1^{2\times 1D}}{\Gamma_1}} \tag{S2.28}$$

where

$$\boxed{p_0^{2\times 1D} = \frac{(Q_{\rm off}+Q_{\rm on})q_{\rm off}}{Z} \text{ and } p_1^{2\times 1D} = \frac{Q_{\rm on}q_{\rm on}}{Z}} \tag{S2.29}$$

are the probabilities to have respectively 0 and 1 bond, $Z = (Q_{\rm off}+Q_{\rm on})q_{\rm off} + Q_{\rm on}q_{\rm on}$ and $\Gamma_0 = \Gamma$ is the friction in the unbound state and $\Gamma_1 = \Gamma + \gamma + k\left(\frac{1}{q_{\rm off}} + \frac{k}{\gamma}\frac{q_{\rm on}}{q_{\rm off}}\right)$ is that contributing to the bound state. A similar result for an N legged caterpillar, simply adapting the probabilities, is thus used to quantify diffusion of DNA-coated colloids on surfaces.

To recover surface only dynamics, one simply has to take $Q_{\rm on}/Q_{\rm off} \to \infty$ in the above expression. In that case one can easily obtain the surface only effective friction Eq. (12) of the main text.

3 List of parameters for typical biological and artificial systems

We give now detailed references and methods to estimate the model parameters: $\Gamma, \gamma, k, q_{\rm on}, q_{\rm off}, N$.

To estimate the reduced tangential hydrodynamic friction near the surface, we calculate $\Gamma = f(\delta/R) \times 6\pi\eta(T)R$ where R is the particle radius and $\eta(T)$ fluid viscosity at the relevant temperature. δ corresponds to the separation distance between the particle and the surface and f is estimated using:

- if $\delta/R > 0.01$, spline interpolation of the data in Ref. [16]; (using Python's scipy.interpolate.splrep)
- if $\delta/R \leq 0.01$, the approximate formula (2.65a) in Ref. [16].

We take $\delta = 2a$ for all DNA-coated colloids and $\delta = a$ for all other systems where a is the length of the linker. As $f(\delta/R)$ varies slowly with δ we can assume that a small error in δ will not affect our results significantly.

For the leg friction we take $\gamma = 6\pi\eta(T)a$.

All other parameters are detailed in the tables below.

Quantity	Range of values	Details
DNA coated colloids - low coverage large colloids		
R	525 nm	Low coverage streptavidin beads of [4]
η	0.0006Pa.s	Viscosity of water at the melting temperature 44 $^\circ C$
a	$10-15$ nm	estimated with for double stranded DNA, 60 nucleotides [17]
k	1×10^{-4} N/m	$k\simeq 3\frac{k_BT}{2Ll_p}$ where $l_p\simeq 3.4$ nm is the typical persistence length corresponding to 10 base pairs in a helix and $L\simeq 60(l_p/10)\simeq 20$ nm [4]
$q_{\rm on}$	2500 $\rm s^{-1}$	from $q_{\rm on}\sim k_{\rm on}\sigma/a\mathcal{N}_{\mathcal{A}}$ with $k_{\rm on}=2.2\times10^6 M^{-1}s^{-1}$ (44.7 $^\circ C$) (value predicted from Ref. [18] for the CCAAGTTATGA sequence used in [4], measurements on sequences with a similar number of bases show slightly lower hybridization rates [19])
$q_{\rm off}$	25000 $\rm s^{-1}$	estimated unbinding rate around the melting temperature with a bound probability of 10% (evaluated using full potential profile estimates following [7]). Expected $q_{\rm off}\simeq q_{\rm on}$ at lower temperatures
σ	$1/(12\,\text{nm}-18\,\text{nm})^2$	coating density [4]
D	1.4×10^{-3} $\mu\rm m^2/s$	at the melting temperature [4]
D_0	0.37 $\mu\rm m^2/s$	calculated as $D_0=k_BT/12\pi\eta R$ with $T=44\,^\circ$C (since close to the surface, longitudinal friction is doubled due to hydrodynamic interactions)
D_0/D	270	diffusion decrease factor, calculated with range of above values
N	$40-70$	estimated from $N\simeq 2\pi Rh\sigma$ taking $h\simeq a/3$ the typical penetration length of the layers, and density limited by the surface density, probably in the lower range $\sigma=1/(16\text{ nm})^2$
$N(T_m)$	40	number of involved legs at the melting point, using the methodology described in Ref. [7]. Taking symmetric (particle and flat surface) density with $\sigma=1/(17\text{ nm})^2$ and the exact DNA sequences and polymer types detailed in Ref. [4]
$D_0/D_{\rm hop}$	$45-800$	calculated with $D_{\rm hop}=D_0q_{\rm off}^N/(q_{\rm off}+q_{\rm on})^N$ with values above.
DNA coated colloids - high coverage large colloids		
R	500 nm	High coverage beads of [7]
η	0.0005Pa.s	Viscosity of water at melting temperatures 50-60 $^\circ C$
a	$13-18$ nm	measured lengths of 6.5 k PEO strands tethered with 20 nucleotides of single stranded DNA [7]
k	2×10^{-4} N/m	$k\simeq 3\frac{k_BT}{2L\ell_p}$ expected spring constant with $\ell_p\simeq 0.5$ nm and $L=80$ nm (mixed brush with PEO and DNA)
$q_{\rm on}$	$1.3-1.9\times10^4$ $\rm s^{-1}$	from $q_{\rm on}\sim k_{\rm on}\sigma/a\mathcal{N}_{\mathcal{A}}$ with $k_{\rm on}=1.6\times10^6 M^{-1}s^{-1}$ (55 $^\circ C$) (value predicted from Ref. [18] for the ACCGCA sequence used in [7])
$q_{\rm off}$	$1.3-1.9\times10^5$ $\rm s^{-1}$	estimated unbinding rate at the melting temperature with a bound probability of 10% (evaluated using full potential profile estimates following [7]). Expected $q_{\rm off}\simeq q_{\rm on}$ at lower temperatures
σ	$1/(3.27\text{ nm})^2$	measured coating density [7]
N	$140-190$	estimated from $N\simeq 2\pi Rh\sigma$ taking $h\simeq a/3$ the typical penetration length of the layers, and density limited by the surface density, probably in the lower range $\sigma=1/(10\text{ nm})^2$

Table S1: Parameter values for DNA coated colloids (large colloids)

Quantity	Range of values	Details
DNA coated nanoparticles		
R	7.5 nm	Gold nanoparticles of Ref. [20]
η	0.0006Pa.s	Viscosity of water at the melting temperature 44 $^{\circ}C$
a	10 nm	Estimated in Ref. [20]
k	2×10^{-4} N/m	$k \simeq 3\frac{k_B T}{2Ll_p}$ where $l_p \simeq 3.4$ nm is the typical persistence length corresponding to 10 base pairs in a helix and $L \simeq 30(l_p/10) \simeq 10$ nm [20]
$q_{\rm on}$	2×10^4 s^{-1}	from $q_{\rm on} \sim k_{\rm on}\sigma/a\mathcal{N}_{\mathcal{A}}$ with $k_{\rm on} = 1.0 \times 10^6 M^{-1}s^{-1}$ (44 $^{\circ}C$) (value predicted from Ref. [18] for the CGCG sequence used in [20])
$q_{\rm off}$	2×10^5 s^{-1}	estimated unbinding rate around the melting temperature with a bound probability of 10% (evaluated using full potential profile estimates following [7]). Expected $q_{\rm off} \simeq q_{\rm on}$ at lower temperatures
σ	$1/(3\text{ nm})^2$	from 80 strands/ 15 nm particle [21]
N	$15-20$	estimated from $N \simeq 2\pi R_{\rm eff} h \sigma_{\rm eff}$ taking $h \simeq a/3$ the typical penetration length of the layers, effective radius of coated nanocolloid $R_{\rm eff} = R + h$ and density at the outer layer $\sigma_{\rm eff} = \sigma R^2/R_{\rm eff}^2$

Table S2: Parameter values for DNA coated nanoparticles

Quantity	Range of values	Details
Leukocyte adhesion mediated by P-selectin or L-selectin		
R	4.15 μm	typical cell size [22]
η	0.001Pa.s	typical physiological conditions [23]
a	300 nm	typical microvillus length [24]
k	$4 \times 10^{-5} - 5 \times 10^{-3}$ N/m	typical spring constant of microvilli [24] up to spring constant of the bond itself (excluding microvilli) [25]
N_b	1-2	typical number of contacts [26, 27]
σ	$15-30$ μm^{-2}	typical density of ligands [28, 27]
N	$40-80$	calculated from $N \simeq 2\pi R h \sigma$ taking $h \simeq a/3$ the typical penetration length of the layers. Coherent with Ref. [29].
P-selectin		
$q_{\rm on}$	$4-300$ s^{-1}	from $q_{\rm on} \sim k_{\rm on}\sigma/a\mathcal{N}_{\mathcal{A}}$ with measured binding rates $k_{\rm on} = (4-100) \times 10^5$ M^{-1}s^{-1} [25, 30, 27]
$q_{\rm off}$	$0.02-1.6$ s^{-1}	measured unbinding rate [25, 30, 23]
L-selectin		
$q_{\rm on}$	$(0.4-4) \times 10^4$ s^{-1}	measured binding rates [26]
$q_{\rm off}$	$7-250$ s^{-1}	measured unbinding rate [31, 28], shorter lifetime than P-selectin

Table S3: Parameter values for white blood cells

Quantity	Range of values	Details
E. Coli motility mediated by adhesion between FimH adhesin at the tip of pili and glycoproteins on the surface		
R	350 nm and $L = 3$ μm	cylindrical features [32]
η	0.001Pa.s	typical physiological conditions [23]
a	100 nm	pili characteristic size to calculate hydrodynamic resistance, from $\sqrt{2L_c\ell}$, see below [33]
k	0.6 μN/m	typical spring constant as $k_BT/L_c\ell$ where $L_c = 2$ μm is the contour length and $\ell = 3.3$ nm is the persistence length [33]
$q_{\rm on}$	$5 - 125$ s^{-1}	from $q_{\rm on} \sim k_{\rm on}\sigma/a\mathcal{N}_{\mathcal{A}}$ with measured binding rates $k_{\rm on} = 2 - 50 \times 10^5$ M^{-1}s^{-1} [34, 35, 36]
$q_{\rm off}$	$1 - 100$ s^{-1}	measured unbinding rate [34, 35, 36]
σ	$15 - 45$ μm^{-2}	Pili density, calculated from 100-300 pili over the cylinder surface [37]
N	$2 - 7$	calculated from $N \simeq 2rL\sigma$ taking $r \simeq \sqrt{2aR/3}$ the typical half width of the cylinder in contact.

Table S4: Parameter values for Escherichia Coli

Quantity	Range of values	Details
Cargo transport by molecular motors		
R	1 μm	typical cargo size [38]
η	0.001Pa.s	typical physiological conditions [23]
a	25 nm	microtubule diameter [39]
k	$0.2 - 0.5$ mN/m	typical spring constant [39, 40]
$q_{\rm on}$	0.4 s^{-1}	measured individual binding rate [41]
$q_{\rm off}$	4 s^{-1}	measured unbinding rate [42]

Table S5: Parameter values for molecular motors

Quantity	Range of values	Details
Protein cargos in the nuclear pore complex		
R	50 nm	estimated from $D = 4$ μm^2/s for karyopherin-β which is a major transporter in the NPC [43, 44], $R = k_BT/6\pi\eta D$, and using η as below
η	0.001Pa.s	typical physiological conditions [23]
a	$8 - 10$ nm	estimated with worm like chain model in [45]
k	0.06-0.1 mN/m	typical spring constant of the Nucleoporin Nup 153 [45]
$q_{\rm on}$	$3\times10^5 - 3\times10^8$ s^{-1}	from $q_{\rm on} \sim k_{\rm on}\rho$ with $k_{\rm on} = 10^7 - 10^9$ M^{-1}s^{-1} [44]
$q_{\rm off}$	$10^4 - 10^7$ s^{-1}	estimated unbinding rate [44]
ρ	$30 - 250$mM	concentration of Nup in pore [44, 46]

Table S6: Parameter values for nuclear pore transport

Quantity	Range of values	Details
Influenza A		
R	60 nm	average measured diameter [47]
η	0.001Pa.s	typical physiological conditions [23]
a	$12-15$ nm	typical height of Hemagglutinin [48, 47]
k	$1-2$ mN/m	typical spring constant [48, 49]
q_{on}	$0.07-130$ s^{-1}	calculated from $q_{\text{on}} \sim q_{\text{off}}/K_D\sigma/a\mathcal{N}_{\mathcal{A}}$ with $K_D = 2-950$ mM [50, 48]
q_{off}	$0.1-30$ s^{-1}	measured unbinding rate (focused on Hemagglutinin to Sialic Acid) [48, 51, 49, 52]
$x = \frac{q_{\text{on}}}{q_{\text{on}}+q_{\text{off}}}$	0.2	Bound fraction at equilibrium [48]
σ	6800 μm^{-2}	average measured coverage of HA proteins on virus (85% of total (HA + NA)) [47]
D	$0.05-0.5$ μm^2/s	measured on typical lipid bilayers with sialic acid receptors [51], strongly dependent on q_{off} in the same qualitative way as predicted in out theory
D	0.01 μm^2/s	also measured on typical surfaces [52]
D_0	1.9 μm^2/s	calculated as $D_0 = k_BT/12\pi\eta R$ with $T = 37\,^\circ$C (since close to the surface, longitudinal friction is doubled due to hydrodynamic interactions)
D_0/D	$4-190$	diffusion decrease factor, calculated with range of above values
N	$10-13$	calculated from $N \simeq 2\pi Rh\sigma$ taking $h \simeq a/3$ the typical penetration length of the layers.
D_0/D_{hop}	$9-20$	calculated with $D_{\text{hop}} = D_0 q_{\text{off}}^N/(q_{\text{off}}+q_{\text{on}})^N$ with values above.
SARS CoV 2		
R	50 nm	typical virus size [53]
η	0.001Pa.s	typical physiological conditions [23]
a	$6-23$ nm	ligand protein characteristic size [54, 53]
k	$0.1-0.4$ N/m	typical spring constant from simulation results [55] and [56]
q_{on}	$770-1500$ s^{-1}	from $q_{\text{on}} \sim k_{\text{on}}\sigma/a\mathcal{N}_{\mathcal{A}}$ with $k_{\text{on}} = 0.7-1.4\times10^5$ M^{-1}s^{-1} [54, 57]
q_{off}	0.05 s^{-1} -0.01 s^{-1}	measured unbinding rate of individual ligand-receptor pairs [55, 54]
N	$1-2$	calculated from $N \simeq 2\pi Rh\sigma$ taking $h \simeq a/3$ the typical penetration length of the layers.
x	0.1-0.2	Bound fraction at equilibrium [54] in AFM experiments
σ	1000 μm^{-2}	density of spike proteins on the surface [53]
SARS CoV 1		
R	50 nm	typical virus size [53]
η	0.001Pa.s	typical physiological conditions [23]
a	$6-23$ nm	ligand protein characteristic size [54, 53]
k	0.6 N/m	typical spring constant from simulation results [55]
q_{on}	$1200-2500$ s^{-1}	from $q_{\text{on}} \sim k_{\text{on}}\sigma/a\mathcal{N}_{\mathcal{A}}$ with $k_{\text{on}} = 0.7-1.4\times10^5$ M^{-1}s^{-1} [54, 57] (similar to Sars CoV 2 [57])
q_{off}	0.6 s^{-1}	measured unbinding rate of individual ligand-receptor pairs [55]
N	$1-4$	calculated from $N \simeq 2\pi Rh\sigma$ taking $h \simeq a/3$ the typical penetration length of the layers.
x	0.1-0.2	Bound fraction at equilibrium is similar to Sars CoV 2 [54, 57]
σ	1600 μm^{-2}	density of spike proteins on the surface [53]

Table S7: Parameter values for viruses

4 Coarse-graining under different models and assumptions

4.1 Coarse-graining with particle inertia

While more details on inertial effects with multivalent receptor contacts will be written in a separate paper [58], here we briefly recapitulate some results of this work to support claims made in the main manuscript.

4.1.1 Equations set up with particle inertia

We consider now that the particle has inertia, described by a mass m. To simplify derivations we can neglect inertial effects from the legs, as in general the legs are much smaller than the particle itself, and hence have much lower mass. Alternatively, in Ref. [58] we will show that one can start with inertia on all components, and take the limit of small mass of the legs relative to particle mass on the final result, and obtain the same result as if the limits were inverted.

We thus write the unbound equations for a particle with a single leg as

$$\begin{cases} \frac{dl}{dt} &= -\frac{k}{\gamma}l + \sqrt{2\frac{k_BT}{\gamma}}\eta_l \\ \frac{dx}{dt} &= v \\ \frac{dv}{dt} &= \frac{1}{m}\left(-\Gamma v + \sqrt{2k_BT\Gamma}\eta_x\right) \end{cases} \tag{S4.1}$$

where m is the mass of the particle and v the velocity of the particle.

When the leg is bound to the surface, it is not necessary to project the dynamics. Writing Newton's second law on the system of the (particle+leg bound to surface) one finds the bound equations

$$\begin{cases} \frac{dl}{dt} &= v \\ \frac{dx}{dt} &= v \\ \frac{dv}{dt} &= \frac{1}{m}\Big[-\Gamma v + \sqrt{2k_BT\Gamma}\eta_x + \left(-\gamma v - kl + \sqrt{2k_BT\gamma}\eta_l\right) \Big] \end{cases}. \tag{S4.2}$$

4.1.2 Possible resolution with particle inertia following Ref. [1]

The generator for the system is

$$\mathcal{L} = \begin{pmatrix} -q_{\rm on} - \frac{k}{\gamma}l\partial_l + \frac{k_BT}{\gamma}\partial_{ll} + v\partial_x - \frac{\Gamma}{m}v\partial_v + \frac{k_BT\Gamma}{m^2}\partial_{vv} & +q_{\rm on} \\ +q_{\rm off} & -q_{\rm off} + v\partial_x + v\partial_l - \frac{k}{m}l\partial_v - \frac{\Gamma+\gamma}{m}v\partial_v + \frac{k_BT(\Gamma+\gamma)}{m^2}\partial_{vv} \end{pmatrix} \tag{S4.3}$$

with a natural stationary distribution (now including a Boltzmann factor corresponding to the kinetic energy of the particle)

$$\pi = \frac{1}{Z}\begin{pmatrix} q_{\rm off}/q_{\rm on} \\ 1 \end{pmatrix} e^{-kl^2/2k_BT} e^{-mv^2/2k_BT}. \tag{S4.4}$$

In addition to non-dimensionalizing space and time we need to non-dimensionalize the velocity. We then take (on top of usual non-dimensional quantities in the paper, reported here for completeness)

$$x \to L_x\tilde{x},\ l \to L\tilde{l},\ t \to \tau\tilde{t}, v \to \tilde{v}L_x/\tau = \tilde{v}\frac{L}{\epsilon}\frac{\epsilon^2 k}{\Gamma}. \tag{S4.5}$$

Mass also needs to be non-dimensionalized. Here we write, following Ref. [1], $m = \tilde{m}Lk\tau^2/L_x$. The dimensionless number $mL_x/(Lk\tau)1/\tau = \tau_v/\tau$ can be interpreted as the ratio of the correlation time of the velocity τ_v to the time scale of observation τ. We require $\tau/\tau_v = \frac{1}{\tilde{m}\epsilon}$ such that we may observe coarse grained

dynamics. Dropping the $\tilde{\cdot}$ notation we find the non-dimensional generator

$$\begin{aligned}\mathcal{L} = \frac{1}{\epsilon^2}\mathcal{L}_0 + \frac{1}{\epsilon}\mathcal{L}_1 + \mathcal{L}_2 =& \frac{1}{\epsilon^2}\begin{pmatrix} -q_{\text{on}} - \frac{\Gamma}{\gamma} l\partial_l + \frac{\Gamma}{\gamma}\partial_{ll} & +q_{\text{on}} \\ +q_{\text{off}} & -q_{\text{off}} \end{pmatrix} + \frac{1}{\epsilon}\begin{pmatrix} 0 & 0 \\ 0 & v\partial_l - \frac{1}{m} l\partial_v \end{pmatrix} \\ &+ \begin{pmatrix} v\partial_x - \frac{1}{m} v\partial_v + \frac{1}{m^2}\partial_{vv} & 0 \\ 0 & v\partial_x - \frac{\Gamma+\gamma}{\Gamma}\frac{1}{m} v\partial_v + \frac{\Gamma+\gamma}{\Gamma}\frac{1}{m^2}\partial_{vv} \end{pmatrix}\end{aligned} \tag{S4.6}$$

We can then set up a similar step by step search of a solution at multiple orders seeking a solution $f = f_0 + \epsilon f_1 + \epsilon f_2 + ...$

At lowest order solving $\mathcal{L}_0 f_0 = 0$ yields simply $f_0 = a(x,t)\begin{pmatrix} 1 \\ 1 \end{pmatrix}$ and the associated equilibrium distribution $\pi_0 = \frac{1}{Z'}\begin{pmatrix} q_{\text{off}}/q_{\text{on}} \\ 1 \end{pmatrix} e^{-l^2/2}$.

At the next order we need to solve $\mathcal{L}_0 f_1 = \frac{l}{m}\partial_v a \begin{pmatrix} 0 \\ 1 \end{pmatrix}$ that is easily shown to yield

$$f_1 = -\frac{1}{1 + \frac{(\gamma+\Gamma)q_{\text{off}}}{\gamma q_{\text{on}} + \Gamma}} \left(\frac{q_{\text{off}}}{q_{\text{on}} + \Gamma/\gamma}\right) \frac{l\partial_v a}{m}. \tag{S4.7}$$

To find a solution at the following order, we need to satisfy the Fredholm alternative $\langle \partial_t f_0 - \mathcal{L}_2 f_0 - \mathcal{L}_1 f_1, \pi_0 \rangle = 0$. Standard algebra yields an equation for the function $a(x,v,t)$ as (back in dimensional scales)

$$\partial_t a = v\partial_x a - \frac{\Gamma^m_{\text{eff}}}{m} v\partial_v a + \frac{k_B T \Gamma^m_{\text{eff}}}{m^2}\partial_{vv} a \tag{S4.8}$$

which corresponds to an inertial motion with friction

$$\boxed{\Gamma^m_{\text{eff}} = \frac{q_{\text{off}}}{q_{\text{on}} + q_{\text{off}}}\Gamma + \frac{q_{\text{on}}}{q_{\text{on}} + q_{\text{off}}}\left(\Gamma + \gamma + k\left(\frac{1}{q_{\text{off}}} + \frac{\gamma}{k}\frac{q_{\text{on}}}{q_{\text{off}}}\right)\right)} \tag{S4.9}$$

which writes with the notations of the main paper

$$\boxed{\Gamma^m_{\text{eff}} = p_0\Gamma_0 + p_1\Gamma_1} \tag{S4.10}$$

which is exactly Eq. (20) of the main paper.

As highlighted in the main paper, there is a notable difference between $\Gamma^m_{\text{eff}} = p_0\Gamma_0 + p_1\Gamma_1$, with inertia, and $\Gamma^{-1}_{\text{eff}} = p_0\Gamma_0^{-1} + p_1\Gamma_1^{-1}$ when inertia is neglected. In particular, the results are not equivalent when unbinding rates are slow such as $q_{\text{off}}\Gamma/k \ll 1$. We will reconcile these results in a separate paper [58].

4.2 Choice of time-scale hierarchy

4.2.1 Averaging with a different choice of scaling $\varepsilon = \gamma/\Gamma$

It is common to assume a different choice of scalings assuming fast unbound tether dynamics. This choice of assumptions can be formulated mathematically as $\gamma/\Gamma = \gamma_r\epsilon^2$, where γ_r is a non-dimensional number of order 1. This typically corresponds to short legs on a large particle, as γ and Γ are expected to scale with leg size and particle size via Stokes law. When doing such a reasoning, it is also common to lighten the assumption on scale separation for x and l and take $L = L_x$ [59]. We keep other non-dimensional scalings. For simplicity we will write $\varepsilon = \epsilon^2$ as no terms in ϵ appear now. We then obtain the non-dimensional

generator as an expansion $\mathcal{L} = \frac{1}{\varepsilon}\mathcal{L}_0 + \mathcal{L}_1 + \varepsilon\mathcal{L}_2 + \varepsilon^2\mathcal{L}_3 + ...$, with the first terms as

$$\mathcal{L} = \frac{1}{\varepsilon}\begin{pmatrix} -q_{\text{on}} - \frac{1}{\gamma_r}l\partial_l + \frac{1}{\gamma_r}\partial_{ll} & q_{\text{on}} \\ q_{\text{off}} & -q_{\text{off}} \end{pmatrix} + \begin{pmatrix} \partial_{xx} & 0 \\ 0 & l(\partial_x - \partial_l) + (\partial_x - \partial_l)^2 \end{pmatrix} + \varepsilon \begin{pmatrix} 0 & 0 \\ 0 & -\gamma_r l(\partial_x - \partial_l) - \gamma_r(\partial_x - \partial_l)^2 \end{pmatrix} + ... \tag{S4.11}$$

Notice above that the non-dimensionalization for the binding rates $q_{\text{on}}, q_{\text{off}}$ is such that it assumes binding and unbinding to be much faster than the long time dynamics searched for.

We look for a solution as $f = f_0 + \varepsilon f_1 + \varepsilon^2 f_2 + ...$ At first order we find easily $f_0 = a(x,t)\begin{pmatrix} 1 \\ 1 \end{pmatrix}$ associated with the equilibrium distribution $\pi_0 \propto \begin{pmatrix} q_{\text{off}}/q_{\text{on}} \\ 1 \end{pmatrix} e^{-l^2/2}$.

At the following order, to find a solution f_1, we require the Fredholm alternative, namely $\langle \partial_t f_0 - \mathcal{L}_1 f_0, \pi_0 \rangle = 0$, yielding

$$\partial_t a - \partial_{xx} a = 0. \tag{S4.12}$$

We can now solve for $\mathcal{L}_0 f_1 = -\mathcal{L}_1 f_0 + \partial_t f_0$ making use of this first order equation on a. The equation to be solved simplifies to $\mathcal{L}_0 f_1 = -\begin{pmatrix} 1 \\ 0 \end{pmatrix} l\partial_x a$. This gives

$$f_1 = \frac{l\partial_x a}{q_{\text{off}}}\begin{pmatrix} \gamma_r q_{\text{on}} \\ 1 + \gamma_r q_{\text{on}} \end{pmatrix}. \tag{S4.13}$$

To solve for f_2 we require the Fredholm alternative at the following order, namely $\langle \partial_t f_0 + \varepsilon\partial_t f_1 - \mathcal{L}_1 f_0 - \varepsilon\mathcal{L}_1 f_1 - \varepsilon\mathcal{L}_2 f_0, \pi_0 \rangle = 0$. We focus on specific terms

$$\langle \partial_t f_1, \pi_0 \rangle = 0, \tag{S4.14}$$

then

$$\langle -\mathcal{L}_1 f_1, \pi_0 \rangle = +\partial_{xx} a \frac{\gamma_r q_{\text{on}} + 1}{q_{\text{off}}}, \tag{S4.15}$$

and

$$\langle -\mathcal{L}_2 f_0, \pi_0 \rangle = +\gamma_r \partial_{xx} a \tag{S4.16}$$

such that summing up all contributions and reverting to original dimensions we obtain

$$\partial_t a = \frac{k_B T}{\Gamma_{\text{eff}}^{\gamma/\Gamma=\varepsilon}} \partial_{xx} a \tag{S4.17}$$

with

$$\boxed{\frac{1}{\Gamma_{\text{eff}}^{\gamma/\Gamma=\varepsilon}} = \left(\frac{q_{\text{off}}}{q_{\text{on}} + q_{\text{off}}}\right)\frac{1}{\Gamma} + \left(\frac{q_{\text{on}}}{q_{\text{on}} + q_{\text{off}}}\right)\frac{1}{\Gamma}\left(1 - \frac{\gamma}{\Gamma}\left[1 + \frac{k}{\gamma}\left(\frac{1}{q_{\text{off}}} + \frac{\gamma}{k}\frac{q_{\text{on}}}{q_{\text{off}}}\right)\right]\right)} \tag{S4.18}$$

with is exactly Eq. (21) of the main paper. We note that this is exactly the γ/Γ first order Taylor expansion of the equation obtained without assuming $\gamma/\Gamma \ll 1$, namely of Eq. (12) of the main paper.

4.2.2 Averaging with pre-averaging of tether dynamics (fast tether relaxation dynamics compared to all other dynamics)

Equation set up with pre-averaging and resolution A commonly used framework is to assume that unbound leg dynamics are so fast that essentially when a new bond is created, the leg length may be sampled from its (bare) equilibrium distribution. This may be formally obtained using homogenization as well by

assuming unbound relaxation is very fast compared to binding dynamics, $\gamma/k \ll 1/q_{\mathrm{on/off}}$, though we do not report the details here. It is a commonly used framework [59, 60].

The unbound state is described by the variables (x,t) while the bound state is described with (x,l,t). We write the equations for the probability distributions in each state

$$\partial_t p_u = -p_u \int e^{-kl^2/2k_BT} q_{\mathrm{on}} dl + \int q_{\mathrm{off}} p_b(x,l,t) dl + \frac{k_BT}{\Gamma} \partial_{xx} p_u \tag{S4.19}$$

$$\partial_t p_b = +p_u e^{-kl^2/2k_BT} q_{\mathrm{on}} + q_{\mathrm{off}} p_b(x,l,t) + \frac{k_BT}{\Gamma+\gamma} \partial_{xx} p_b + (...) \tag{S4.20}$$

where the (...) denote the rest of the bound projected dynamics and Z is some normalization constant that does not depend on l. Notice that here we kept the $\Gamma+\gamma$ in the bound state to highlight that such a term would have to be kept in the case of a great number of springs N, as this would become $\Gamma + N\gamma$ and would therefore have to remain. The equilibrium distribution associated with these dynamics is simply $\pi = \frac{1}{Z}\begin{pmatrix} \frac{q_{\mathrm{off}}}{q_{\mathrm{on}}} \\ e^{-\beta k l^2} \end{pmatrix}$ and satisfies detailed balance:

$$\pi_u \times q_{\mathrm{on}} e^{-\beta k l^2/2} = \frac{1}{Z}\frac{q_{\mathrm{off}}}{q_{\mathrm{on}}} \times q_{\mathrm{on}} e^{-\beta k l^2/2} = \frac{e^{-\beta k l^2/2}}{Z} \times q_{\mathrm{off}} = \pi_b \times q_{\mathrm{off}}. \tag{S4.21}$$

With this approach (compared to the main paper derivation), the only part of the generator that changes is the lowest order term $\mathcal{L}_0$. In particular one should determine the non-dimensionalization. Importantly here one should notice that q_{on} and q_{off} do not have the same units. The ratio $q_{\mathrm{off}}/q_{\mathrm{on}} = O(L)$ has units of a lengthscale. We can therefore keep the usual non-dimensionalization for $q_{\mathrm{off}}\frac{\Gamma}{k\epsilon^2} = \frac{\tilde{q_{\mathrm{off}}}}{\epsilon^2}$ but not for the binding rate, which we take as $q_{\mathrm{on}}\frac{\Gamma}{kL\epsilon^2} = \frac{\tilde{q_{\mathrm{on}}}}{\epsilon^2}$. We find (dropping the $\tilde{\cdot}$)

$$\mathcal{L}_0 = \begin{pmatrix} -\int q_{\mathrm{on}} e^{-l^2/2} dl & +\int q_{\mathrm{on}} e^{-l^2/2} dl \\ +q_{\mathrm{off}} & -q_{\mathrm{off}} - l\partial_l + \partial_{ll}. \end{pmatrix} \tag{S4.22}$$

Resolution for f_0 does not change and we get $f_0 = a(x,t)\begin{pmatrix} 1 \\ 1 \end{pmatrix}$, with associated equilibrium distribution $\pi_0 = \pi$.

At the next order we get the solution $f_1 = l\partial_x a \frac{1}{1+q_{\mathrm{off}}}\begin{pmatrix} 0 \\ 1 \end{pmatrix}$.

Finally at second order we require the Fredholm alternative $\langle \partial_t f_0 - \mathcal{L}_2 f_0 - \mathcal{L}_1 f_1, \pi_0 \rangle = 0$ yielding

$$\partial_t a = \frac{k_BT}{\Gamma_{\mathrm{eff}}^{\mathrm{k}/\gamma \gg \mathrm{q}}} \partial_{xx} a \tag{S4.23}$$

with

$$\boxed{\frac{1}{\Gamma_{\mathrm{eff}}^{\mathrm{k}/\gamma \gg \mathrm{q}}} = \left(\frac{q_{\mathrm{off}}}{q_{\mathrm{on}}+q_{\mathrm{off}}}\right)\frac{1}{\Gamma} + \left(\frac{q_{\mathrm{on}}}{q_{\mathrm{on}}+q_{\mathrm{off}}}\right)\frac{1}{\Gamma+\gamma+\frac{k}{q_{\mathrm{off}}}}.} \tag{S4.24}$$

This is nearly exactly the result obtained without pre-averaging but for the $k\tau_{\mathrm{u}}^{\mathrm{relax}} = k\left(\frac{\gamma}{k}\frac{q_{\mathrm{on}}}{q_{\mathrm{off}}}\right)$ contribution corresponding to the time the tether is allowed to relax between 2 binding periods. It is exactly the result reported in Eq. (22) of the main manuscript.

Relation to Ref. [12] In this paragraph we relate our results to the results obtained in Ref. [12]. Eq. (2.48) of Ref. [12] finds an effective long time diffusion, starting from similar equations as Eq. (S4.20),

$$D_{\mathrm{eff}}^{\text{Ref. [12]}} = D_0\left(1 + \varepsilon\frac{\nu-2}{\beta_0(1+\beta_0)\lambda}\right) \tag{S4.25}$$

where we will give the meaning of the new notations (ν, ε, β_0, λ) by expressing them with respect to our notations. Here, $\nu = k/k_{\text{tether}} = 1$ in our case because there is no change in recall spring force between the bound (k_{tether}) and unbound states (k). We also have $\beta_0 = \frac{q_{\text{off}}}{q_{\text{on}}}$, here $\varepsilon = \frac{D_0}{q_{\text{on}} L^2}$ and $\lambda = k_B T/kL^2$ such that the effective diffusion writes with our notations

$$D_{\text{eff}}^{\text{Ref. [12]}} = D_0 \left(1 - \frac{k/q_{\text{off}}}{\Gamma} \frac{q_{\text{on}}}{q_{\text{on}} + q_{\text{off}}}\right). \tag{S4.26}$$

Compared to the previous derivation, this result corresponds to an effective friction with pre-averaging of tether dynamics (which is indeed what is done in Ref. [12]) *and* scales with k/q_{off} similarly as the derivation assuming $\gamma/\Gamma = \varepsilon$. In Ref. [12], as the dynamics are already pre-averaged, they are expressed at 0^{th} order in γ/Γ. Therefore the key common point of these derivations (Ref. [12] and Sec. 2.2 here) is to assume similar spatial scales, namely $L_x = L$. This highlights that the assumption $L/L_x = \epsilon$ allows one to "safely" average dynamics without specific assumptions on other physical parameters.

Relation to N legs facing a uniformly sticky membrane In Fig. S6 we show that the pre-averaged result corresponds to the predictions for N legs facing a uniformly sticky surface when the average number of bonds legs $N_b \lesssim 1$.

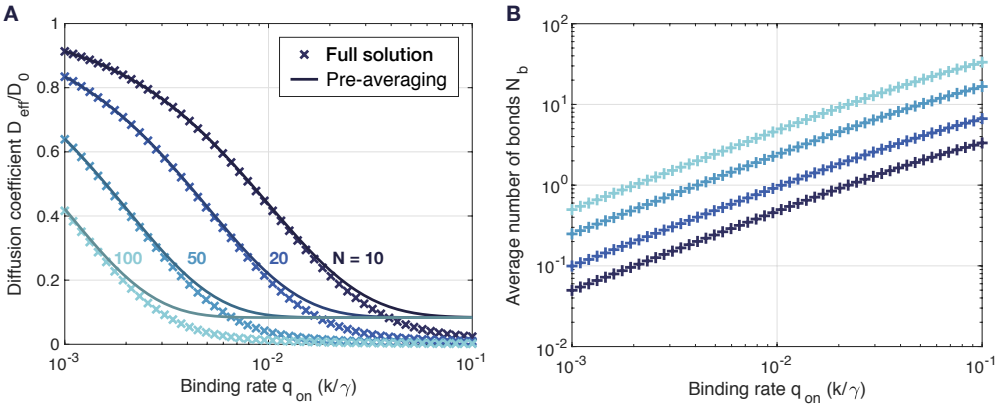

Figure S6: Pre-averaged results correspond to N legs facing a uniformly sticky surface when the average number of bonds legs $N_b \lesssim 1$. (A) D_{eff} as calculated with a numerical resolution of Eq. (15) of the main paper ("Full solution") or with the pre-averaged result of Eq. (22) of the main paper ("Pre-averaging") with respect to the binding rate q_{on}. Other parameters are $\frac{\gamma}{\Gamma} = 1$ and $\frac{q_{\text{off}}\Gamma}{k} = 0.1$; (B) Corresponding average number of bonds N_b.

4.2.3 Averaging with fast binding dynamics compared to relaxation dynamics

To understand how fast binding dynamics affect this system, we use the same non-dimensionalization as in the main text but for $L = L_x$ (thereby allowing relaxation dynamics to be of similar order as the long time mobility of the particle). We obtain the non-dimensional generator

$$\mathcal{L} = \frac{1}{\epsilon^2}\begin{pmatrix} -q_{\text{on}} & q_{\text{on}} \\ q_{\text{off}} & -q_{\text{off}} \end{pmatrix} + \begin{pmatrix} \frac{\Gamma}{\gamma}\left(-l\partial_l + \partial_{ll}\right) + \partial_{xx} & 0 \\ 0 & \frac{\Gamma}{\Gamma+\gamma}\left(l(\partial_x - \partial_l) + (\partial_x - \partial_l)^2\right) \end{pmatrix} = \frac{1}{\varepsilon}\mathcal{L}_0 + \mathcal{L}_1 \tag{S4.27}$$

where we used $\varepsilon = \epsilon^2$.

We then seek a solution as an expansion $f = f_0 + \varepsilon f_1 + \varepsilon^2 f_2 + ...$ At lowest order we need to solve

$$\begin{pmatrix} -q_{\text{on}} & q_{\text{on}} \\ q_{\text{off}} & -q_{\text{off}} \end{pmatrix} f_0 = 0 \tag{S4.28}$$

which simply yields $f_0 = a(x,l,t)\begin{pmatrix}1\\1\end{pmatrix}$ and the associated equilibrium distribution $\pi_0 = \begin{pmatrix}\frac{q_{\rm off}}{q_{\rm on}}\\1\end{pmatrix}$. Notice how here the equilibrium distribution at lowest order does not correspond to the full equilibrium distribution $\pi_0 \neq \pi$. At the following order to find a solution to the problem we require the Fredholm alternative $\langle \partial_t f_0 - \mathcal{L}_1 f_0, \pi_0\rangle = 0$, which gives the equation

$$\begin{aligned}\partial_t a =& p_0 \frac{\Gamma}{\gamma}\left(-l\partial_l + \partial_{ll}\right) + p_0\partial_{xx} \\ &+ p_1 \frac{\Gamma}{\Gamma+\gamma}\left(l(\partial_x - \partial_l) + (\partial_x - \partial_l)^2\right)\end{aligned} \tag{S4.29}$$

where $p_0 = \frac{q_{\rm off}}{q_{\rm off}+q_{\rm on}} = 1 - p_1$ is the probability to be unbound and p_1 to be bound. This new effective equation can now be explored by means of time and length scale separation by setting a new small scale parameter $\epsilon_2 = \frac{L}{L_x}$. This small scale operator allows us to write

$$\partial_t a = \frac{1}{\epsilon_2^2}\mathcal{L}_{0,2} + \frac{1}{\epsilon_2}\mathcal{L}_{1,2} + \mathcal{L}_{2,2} \tag{S4.30}$$

where $\mathcal{L}_{0,2} = \left(p_0\frac{\Gamma}{\gamma} + p_1\frac{\Gamma}{\Gamma+\gamma}\right)\left(-l\partial_l + \partial_{ll}\right)$, $\mathcal{L}_{1,2} = p_1\frac{\Gamma}{\Gamma+\gamma}\left(l\partial_x - 2\partial_{xl}\right)$ and $\mathcal{L}_{2,2} = \left(p_0 + p_1\frac{\Gamma}{\Gamma+\gamma}\right)\partial_{xx}$. We seek a solution $a = a_0 + \epsilon_2 a_1 + \epsilon_2^2 a_2 + ...$

At lowest order we need to solve $\mathcal{L}_{0,2}a_0 = 0$ which implies $a_0 = a_0(x,t)$ making use of vanishing flux boundary conditions at infinity. The associated equilibrium distribution is now $\pi_{0,2} = e^{-l^2/2}/Z$.

At the next order we need to solve $\mathcal{L}_{0,2}a_1 = -\mathcal{L}_{1,2}f_0 = -p_1\frac{\Gamma}{\Gamma+\gamma}l\partial_x a$ such that $a_1 = -\frac{p_1\frac{\Gamma}{\Gamma+\gamma}}{p_0\frac{\Gamma}{\gamma}+p_1\frac{\Gamma}{\Gamma+\gamma}}l\partial_x a = -\frac{l\partial_x a}{1+\frac{p_0}{p_1}\frac{\gamma}{\Gamma+\gamma}}$. At the following order, to find a solution we require the Fredholm alternative, namely $\langle \partial_t a_0 - \mathcal{L}_{2,2}a_0 - \mathcal{L}_{1,2}a_1, \pi_{0,2}\rangle = 0$. After some standard algebra one finds

$$\partial_t a_0 = \frac{1}{\Gamma^{q\,\rm fast}}\partial_{xx}a \tag{S4.31}$$

where

$$\frac{1}{\Gamma^{q\,\rm fast}} = \frac{p_0}{\Gamma} + \frac{p_1}{\Gamma + \gamma/p_0} \tag{S4.32}$$

which, reverting to dimensional scales, is exactly Eq. (23) of the main paper.

4.3 Arm and/or legs

4.3.1 Arm or leg

In this part we show precisely how having an arm (spring always attached to the surface) or a leg (spring always attached to the particle) affects the dynamics. There are several ways one can consider to obtain the dynamics of the leg or the arm (referred to henceforth as spring). Either assume (1) that the center of mass of the spring is attached to the particle (or the surface), (2) either that the center of mass is located at the free end of the spring (when it is attached to the particle or the surface). Both assumptions do not yield exactly the same dynamics but the differences in the long time effective dynamics are minor.

(1) Arm or leg (spring) attached by their center of mass Consider in general a free spring, where motion is confined to a line but none of the spring ends are attached. The length of the spring l (more accurately here l represents the length imbalance compared to the rest length of the spring $l - l_0$ but we take $l_0 = 0$ for simplicity) obeys the overdamped Langevin equation

$$\frac{dl}{dt} = -\frac{kl}{\gamma} + \sqrt{\frac{2k_BT}{\gamma}}\eta_l. \tag{S4.33}$$

The center of mass c of the spring similarly obeys an overdamped Langevin equation, with diffusion only

$$\frac{dc}{dt} = \sqrt{\frac{2k_BT}{\gamma}}\eta_c \tag{S4.34}$$

and we considered that the diffusion coefficient of the center of mass is similar to that of the spring length. For simplicity we consider here that the center of mass of the spring is located at one of its ends, namely the end that will be permanently attached to a surface in this paragraph.

In addition the particle also diffuses as

$$\frac{dx}{dt} = \sqrt{\frac{2k_BT}{\Gamma}}\eta_x. \tag{S4.35}$$

Arm configuration. If we consider the arm configuration, then the center of mass c is attached to the surface and satisfies the constraint $q(x, l, c) = c - x_{\text{surface}} = 0$. The projected dynamics in that case are trivial and sum up to the ones detailed in the main text and recalled here for consistency:

$$\begin{cases} \frac{dx}{dt} = \sqrt{\frac{2k_BT}{\Gamma}}\eta_x, \\ \frac{dl}{dt} = -\frac{kl}{\gamma} + \sqrt{\frac{2k_BT}{\gamma}}\eta_l, \\ \frac{dc}{dt} = 0. \end{cases} \tag{S4.36}$$

Leg configuration. If we consider the leg configuration, then the center of mass c is attached to the particle and satisfies the constraint $q(x, l, c) = x - c = 0$. This constraint is similar to the one for the bound spring for which the projection formalism is described in Appendix A of the main text. The projected dynamics are therefore

$$\begin{cases} \frac{dx}{dt} = \sqrt{\frac{2k_BT}{\Gamma+\gamma}}\eta_x, \\ \frac{dl}{dt} = -\frac{kl}{\gamma} + \sqrt{\frac{2k_BT}{\gamma}}\eta_l, \\ \frac{dc}{dt} = \frac{dx}{dt}. \end{cases} \tag{S4.37}$$

These dynamics are exactly equivalent to the arm configuration but for the change $\Gamma \to \Gamma + \gamma$, and therefore yield the same resulting effective long time dynamics with a similar change $\Gamma \to \Gamma + \gamma$. One can thus simply consider that Γ is indeed the friction coefficient of the unbound particle, which potentially includes corrections to friction due to legs being attached to the surface.

(2) Arm or leg (spring) with center of mass at the free end We now consider the situation where the center of mass of the spring is located at its free end, and the other end is attached to the particle or the surface.

Leg configuration. Consider in general a spring, attached to one end to the particle (in x) and to the other end to the spring's mass (in $x+l$). Newton's second law on each mass, and taking loosely overdamped dynamics with masses going to 0, yields the system of equations

$$\begin{cases} 0 &= -\Gamma\frac{dx}{dt} + kl + \sqrt{2k_BT\Gamma}\eta_x, \\ 0 &= -\gamma\frac{d(x+l)}{dt} - kl + \sqrt{2k_BT\gamma}\eta_l. \end{cases} \tag{S4.38}$$

The system simplifies for each variable into

$$\begin{cases} \frac{dx}{dt} = +\frac{kl}{\Gamma} + \sqrt{\frac{2k_BT}{\Gamma}}\eta_x, \\ \frac{dl}{dt} = -kl\left(\frac{1}{\Gamma} + \frac{1}{\gamma}\right) - \sqrt{\frac{2k_BT}{\Gamma}}\eta_x + \sqrt{\frac{2k_BT}{\gamma}}\eta_l. \end{cases} \tag{S4.39}$$

This system corresponds to a friction matrix and force field

$$\tilde{\Gamma}^{-1} = \begin{pmatrix} \frac{1}{\Gamma} & -\frac{1}{\Gamma} \\ -\frac{1}{\Gamma} & \frac{1}{\gamma} + \frac{1}{\Gamma} \end{pmatrix} \text{ and } \nabla\mathcal{U} = \begin{pmatrix} 0 \\ kl \end{pmatrix}. \tag{S4.40}$$

When the spring (here the leg) becomes temporarily bound to the surface, the bound equations then simply read (provided appropriate projection, following Appendix A, is made)

$$\begin{cases} \frac{dx}{dt} = +\frac{kl}{\Gamma} + \sqrt{\frac{2k_BT}{\Gamma}}\eta_x, \\ \frac{dl}{dt} = -\frac{dx}{dt} = -\frac{kl}{\Gamma} - \sqrt{\frac{2k_BT}{\Gamma}}\eta_x. \end{cases} \tag{S4.41}$$

In non-dimensional scales, the hierarchy of generators now reads

$$\mathcal{L}_0 = \begin{pmatrix} -q_{\text{on}} + \frac{\Gamma+\gamma}{\Gamma}\left(-l\partial_l + \partial_{ll}\right) & q_{\text{on}} \\ q_{\text{off}} & q_{\text{off}} + \left(-l\partial_l + \partial_{ll}\right) \end{pmatrix}, \tag{S4.42}$$

$$\mathcal{L}_1 = \begin{pmatrix} (l\partial_x - 2\partial_{lx}) & 0 \\ 0 & (l\partial_x - 2\partial_{lx}) \end{pmatrix}, \text{ and } \mathcal{L}_2 = \begin{pmatrix} \partial_{xx} & 0 \\ 0 & \partial_{xx} \end{pmatrix}. \tag{S4.43}$$

Using a coarse-graining method as usual, we obtain simply the usual harmonic sum $\Gamma_{\text{eff}}^{-1} = p_0\Gamma_0^{-1} + p_1\Gamma_1^{-1}$ where the friction coefficients write

$$\begin{cases} \Gamma_0 = & \Gamma + \gamma + k\left(\frac{\gamma}{k}\frac{q_{\text{on}}}{q_{\text{off}}+k/\Gamma}\right) \\ \Gamma_1 = & \Gamma + \gamma + k\left(\frac{1}{q_{\text{off}}} + \frac{\gamma}{k}\frac{q_{\text{on}}+k/\Gamma}{q_{\text{off}}}\right) \text{ (model (2))}. \end{cases} \tag{S4.44}$$

Compared to the coefficients obtained if the spring is attached to the particle by its center of mass (model (1)), namely

$$\begin{cases} \Gamma_0 = & \Gamma + \gamma \\ \Gamma_1 = & \Gamma + \gamma + k\left(\frac{1}{q_{\text{off}}} + \frac{\gamma}{k}\frac{q_{\text{on}}+q_{\text{off}}}{q_{\text{off}}}\right), \text{ (model (1))}, \end{cases} \tag{S4.45}$$

the results are quite similar independent of the attaching model. Qualitatively, in the non-center of mass case (model (2)), we obtain additional feedback friction terms due to the spring, as $k\tau_{\text{eff}}$ where τ_{eff} is a typical time over which the spring relaxes, scaling naturally as γ/k multiplied by a ratio of characteristic times $\frac{\tau_{\dots}}{\tau_{\dots}}$. This ratio corresponds to the fact that the spring may only relax in the other state, and hence different ratios appear according to the different modeling options and bound states. Be that as it may, such contributions are generally minor. In fact, one can verify (not shown here) that the numerical values of $\Gamma_{\text{eff}}/\Gamma$ according to model (1) or (2) show very little difference over full $\mathbb{R}^3$ space described by the parameters.

We now explore potential differences when the number of legs is increased. For 2 legs, the dynamics in the unbound state are

$$\begin{cases} \frac{dx}{dt} = +\frac{k(l_1+l_2)}{\Gamma} + \sqrt{\frac{2k_BT}{\Gamma}}\eta_x, \\ \frac{dl_1}{dt} = -\frac{dx}{dt} - \frac{kl_1}{\gamma} + \sqrt{\frac{2k_BT}{\gamma}}\eta_1 \\ \frac{dl_2}{dt} = -\frac{dx}{dt} - \frac{kl_2}{\gamma} + \sqrt{\frac{2k_BT}{\gamma}}\eta_2 \end{cases} \tag{S4.46}$$

and when leg 1 is bound to the surface simply

$$\begin{cases} \frac{dx}{dt} = -\frac{dl_1}{dt} = +\frac{k(l_1+l_2)}{\Gamma} + \sqrt{\frac{2k_BT}{\Gamma}}\eta_x, \\ \frac{dl_2}{dt} = -\frac{dx}{dt} - \frac{kl_2}{\gamma} + \sqrt{\frac{2k_BT}{\gamma}}\eta_2 \end{cases} \tag{S4.47}$$

and when both legs are bound

$$\left\{ \frac{dx}{dt} = -\frac{dl_1}{dt} = -\frac{dl_2}{dt} = +\frac{k(l_1+l_2)}{\Gamma} + \sqrt{\frac{2k_BT}{\Gamma}}\eta_x. \right. \tag{S4.48}$$

Dynamics are then easily extended to N legs using the free spring end model applied to each leg. Coarse-graining and asymptotics (around the average number of bonds) then easily lead to

$$\Gamma_{\text{eff}} \simeq \Gamma_{N_b} = \Gamma + N\gamma + N_b\left[\gamma + k\left(\frac{1}{q_{\text{off}}} + \frac{\gamma}{k}\frac{q_{\text{on}}}{q_{\text{off}}}\right)\right] \text{ (model (2))}. \tag{S4.49}$$

Eq. (S4.49) is exactly the result obtained by attaching legs by their center of mass (model (1)), provided the suitable change $\Gamma \to \Gamma + N\gamma$ is done for N legs. There is thus no difference between the different models in the leg configuration when a large number of legs are involved.

Arm configuration. The arm configuration with mass at the free end (model (2)) is trivially equivalent to that attached by the center of mass as

$$\begin{cases} \frac{dx}{dt} = \sqrt{\frac{2k_BT}{\Gamma}}\eta_x, \\ \frac{dl}{dt} = -\frac{kl}{\gamma} + \sqrt{\frac{2k_BT}{\gamma}}\eta_l. \end{cases} \tag{S4.50}$$

There is thus no difference between the different models in the arm configuration.

4.3.2 Arm and leg

Equations set up We consider random attachement and detachement of two springs to one another, in the leg and arm geometry – see Fig. S7-A.

When the springs are unbound the dynamic equations are

$$\begin{cases} \frac{dl_1}{dt} &= -\frac{k}{\gamma}l_1 + \sqrt{\frac{2k_BT}{\gamma}}\eta_1(t) \\ \frac{dl_2}{dt} &= -\frac{k}{\gamma}l_2 + \sqrt{\frac{2k_BT}{\gamma}}\eta_2(t) \\ \frac{dx}{dt} &= \sqrt{\frac{2k_BT}{\Gamma}}\eta_x(t) \end{cases} \tag{S4.51}$$

where l_1 is the length of the top spring, l_2 the length of the bottom spring, and for simplicity here we took $l_0 = 0$.

In the bound state we need to project the dynamics. When the springs bind, we consider that a rigid bond is formed between the springs' sticky ends that keeps the distance constant – see Fig. S7. The dynamic constraint is then

$$q(x, l_1, l_2) = x + l_1 - l_2 + l_{\text{bond}} = 0 \tag{S4.52}$$

where l_{bond} is the length of the bond and remains constant until the springs detach and reattach to form another bond length. If we imagine that the bottom spring is part of a periodic array of springs, such that at any time, only one bottom spring is accessible to the top spring, l_{bond} is typically of order L – see Fig. S7 – and thus a reasonable physical assumption.

The constraint matrix is then $C = (1, 1, -1)$ and the projection matrix

$$P = 1 - \frac{1}{3}\begin{pmatrix} 1 & 1 & -1 \\ 1 & 1 & -1 \\ -1 & -1 & 1 \end{pmatrix} = \frac{1}{3}\begin{pmatrix} 2 & -1 & 1 \\ -1 & 2 & 1 \\ 1 & 1 & 2 \end{pmatrix} \tag{S4.53}$$

such that the Moore-Penrose pseudo inverse of the projected friction is

$$\Gamma_P^\dagger = \frac{1}{\gamma + 2\Gamma}\begin{pmatrix} 2 & -1 & 1 \\ -1 & \frac{\gamma+\Gamma}{\gamma} & \frac{\Gamma}{\gamma} \\ 1 & \frac{\Gamma}{\gamma} & \frac{\gamma+\Gamma}{\gamma} \end{pmatrix} \tag{S4.54}$$

with a square root

$$\sigma_P = \frac{1}{\gamma + 2\Gamma}\begin{pmatrix} 2\sqrt{\Gamma} & \sqrt{\gamma} & -\sqrt{\gamma} \\ \sqrt{\Gamma} & \sqrt{\gamma}/2 + \frac{\gamma+2\Gamma}{\sqrt{4\gamma}} & -\sqrt{\gamma}/2 + \frac{\gamma+2\Gamma}{\sqrt{4\gamma}} \\ -\sqrt{\Gamma} & -\sqrt{\gamma}/2 + \frac{\gamma+2\Gamma}{\sqrt{4\gamma}} & \sqrt{\gamma}/2 + \frac{\gamma+2\Gamma}{\sqrt{4\gamma}} \end{pmatrix}. \tag{S4.55}$$

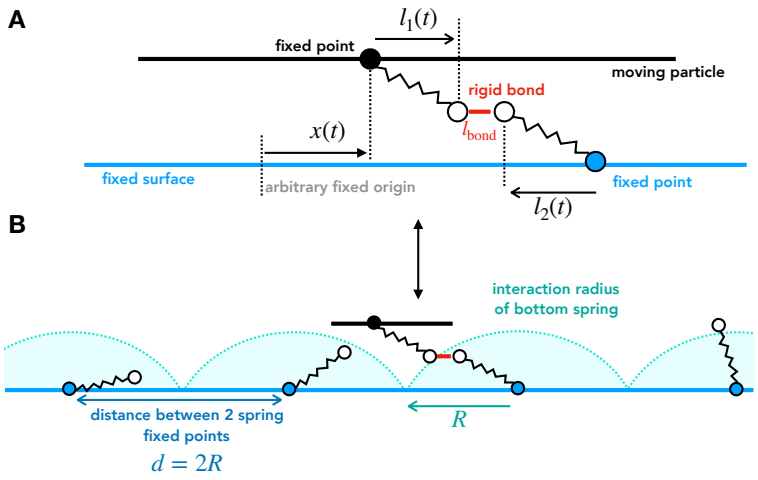

Figure S7: Geometry of binding with a particle having an arm and a leg. (A) The spring attached to the moving particle may bind to the bottom spring by forming a rigid bond that "fills in the distance" between the separated springs. Such a model is equivalent to (B) where the bond is formed with the "closest" available bond. Here if springs on the surface are evenly spaced with a typical spacing $d = 2R$ we consider that the top spring's sticky end binds to a surface spring whose fixed point is closest, and always closer than R. Switching events between one spring and then another are long if the distance between two surface springs is large and are ignored. The equivalence between A and B could be shown more systematically, but is beyond the scope of this manuscript.

The dynamics in the bound state are therefore

$$\begin{cases} \frac{dx}{dt} &= -\frac{k}{2\Gamma+\gamma}(l_1-l_2) + \sqrt{\frac{8k_BT\Gamma}{(2\Gamma+\gamma)^2}}\eta_x + \sqrt{\frac{2k_BT\gamma}{(2\Gamma+\gamma)^2}}(\eta_1-\eta_2) \\ \frac{dl_1}{dt} &= \frac{1}{2}\frac{dx}{dt} - \frac{k}{2\gamma}(l_1+l_2) + \sqrt{\frac{2k_BT}{4\gamma}}(\eta_1+\eta_2) \\ \frac{dl_2}{dt} &= -\frac{1}{2}\frac{dx}{dt} - \frac{k}{2\gamma}(l_1+l_2) + \sqrt{\frac{2k_BT}{4\gamma}}(\eta_1+\eta_2) \end{cases} \tag{S4.56}$$

Generator The generator is then

$$\begin{aligned} \mathcal{L} = &\begin{pmatrix} -q_{\text{on}} & q_{\text{on}} \\ q_{\text{off}} & -q_{\text{off}} \end{pmatrix} + \begin{pmatrix} -\frac{k}{\gamma}l_1\partial_{l_1} + \frac{k_BT}{\gamma}\partial_{l_1l_1} - \frac{k}{\gamma}l_2\partial_{l_2} + \frac{k_BT}{\gamma}\partial_{l_2l_2} + \frac{k_BT}{\Gamma}\partial_{xx} & 0 \\ 0 & 0 \end{pmatrix} \\ &+ \begin{pmatrix} 0 & 0 \\ 0 & -\frac{k}{2\Gamma+\gamma}(l_1-l_2)(\partial_x - \frac{1}{2}\partial_{l_2} + \frac{1}{2}\partial_{l_1}) - \frac{k}{2\gamma}(l_1+l_2)(\partial_{l_2}+\partial_{l_1}) \end{pmatrix} \\ &+ \begin{pmatrix} 0 & 0 \\ 0 & +\frac{2k_BT}{2\Gamma+\gamma}(\partial_x - \frac{1}{2}\partial_{l_2} + \frac{1}{2}\partial_{l_1})^2 + \frac{k_BT}{2\gamma}(\partial_{l_2}+\partial_{l_1})^2 \end{pmatrix} \end{aligned} \tag{S4.57}$$

With this generator one can check that $\mathcal{L}^\star\pi = 0$ with the natural equilibrium distribution

$$\pi = \frac{1}{Z}\begin{pmatrix} q_{\text{off}}/q_{\text{on}} \\ 1 \end{pmatrix} e^{-kl_1^2/2k_BT} e^{-kl_2^2/2k_BT} \tag{S4.58}$$

where Z is a normalization constant.

Homogenization Taking the usual scalings we get the following non-dimensional, expanded generator

$$\begin{aligned}\mathcal{L} =&\frac{1}{\epsilon^2}\Bigg[\begin{pmatrix}-q_{\text{on}} & q_{\text{on}}\\ q_{\text{off}} & -q_{\text{off}}\end{pmatrix}+\frac{\Gamma}{\gamma}\begin{pmatrix}-l_1\partial_{l_1}+\partial_{l_1l_1}-l_2\partial_{l_2}+\partial_{l_2l_2} & 0\\ 0 & 0\end{pmatrix}\\ &+\begin{pmatrix}0 & 0\\ 0 & -\frac{\Gamma}{2(2\Gamma+\gamma)}(l_1-l_2)(\partial_{l_1}-\partial_{l_2})-\frac{\Gamma}{2\gamma}(l_1+l_2)(\partial_{l_2}+\partial_{l_1})+\frac{\Gamma}{2(2\Gamma+\gamma)}(\partial_{l_2}-\partial_{l_1})^2+\frac{\Gamma}{2\gamma}(\partial_{l_2}+\partial_{l_1})^2\end{pmatrix}\Bigg]\\ &+\frac{1}{\epsilon}\begin{pmatrix}0 & 0\\ 0 & -\frac{\Gamma}{2\Gamma+\gamma}(l_1-l_2)\partial_x+\partial_x(\partial_{l_1}-\partial_{l_2})\frac{2\Gamma}{\gamma+2\Gamma}\end{pmatrix}\\ &+1\begin{pmatrix}\partial_{xx} & 0\\ 0 & \frac{2\Gamma}{\gamma+2\Gamma}\partial_{xx}\end{pmatrix}=\frac{1}{\epsilon^2}\mathcal{L}_0+\frac{1}{\epsilon}\mathcal{L}_1+\mathcal{L}_2\end{aligned} \tag{S4.59}$$

We now seek an expanded solution f of $\partial_t f=\mathcal{L}f$ as $f=f_0+\epsilon f_1+\epsilon^2 f_2+...$

At lowest order, $\mathcal{L}_0 f_0=0$ gives $f_0=a(x,t)\begin{pmatrix}1\\1\end{pmatrix}$, and the associated equilibrium distribution $\pi_0=\pi$. At first order we need to solve

$$\mathcal{L}_0 f_1=-\mathcal{L}_1 f_0=+\begin{pmatrix}0\\1\end{pmatrix}\frac{\Gamma}{\gamma+2\Gamma}(l_1-l_2)\partial_x a \tag{S4.60}$$

which has a unique solution

$$f_1=-\begin{pmatrix}\frac{\gamma q_{\text{on}}}{\Gamma+\gamma q_{\text{on}}}\\1\end{pmatrix}\frac{(l_1-l_2)\partial_x a}{1+\frac{\Gamma q_{\text{off}}}{\Gamma+\gamma q_{\text{on}}}\frac{\gamma+2\Gamma}{\Gamma}}. \tag{S4.61}$$

At 2nd order we need to satisfy the Fredholm alternative $\langle\partial_t f_0-\mathcal{L}_2 f_0-\mathcal{L}_1 f_1,\pi_0\rangle=0$. We split up the terms to highlight calculation steps (discarding Z terms to simplify notations, as they would cancel out eventually)

$$\begin{aligned}\langle\mathcal{L}_1 f_1,\pi_0\rangle=&-\langle\left(-(l_1-l_2)^2\frac{\Gamma}{\gamma+2\Gamma}+2\frac{2\Gamma}{\gamma+2\Gamma}\right)e^{-l_1^2/2}e^{-l_2^2/2}\rangle\frac{\partial_{xx}a}{1+\frac{\Gamma q_{\text{off}}}{\Gamma+\gamma q_{\text{on}}}\frac{\gamma+2\Gamma}{\Gamma}}\\ =&-\left(-2\frac{\Gamma}{\gamma+2\Gamma}+2\frac{2\Gamma}{\gamma+2\Gamma}\right)\frac{\partial_{xx}a}{1+\frac{\Gamma q_{\text{off}}}{\Gamma+\gamma q_{\text{on}}}\frac{\gamma+2\Gamma}{\Gamma}}\\ =&-\frac{2\Gamma}{\gamma+2\Gamma}\frac{\partial_{xx}a}{1+\frac{\Gamma q_{\text{off}}}{\Gamma+\gamma q_{\text{on}}}\frac{\gamma+2\Gamma}{\Gamma}}\end{aligned} \tag{S4.62}$$

and

$$\langle\mathcal{L}_2 f_0,\pi_0\rangle=\left(\frac{q_{\text{off}}}{q_{\text{on}}}+\frac{2\Gamma}{\gamma+2\Gamma}\right)\partial_{xx}a. \tag{S4.63}$$

Gathering terms as $\langle\partial_t f_0,\pi_0\rangle=\langle\mathcal{L}_2 f_0,\pi\rangle+\langle\mathcal{L}_1 f_1,\pi_0\rangle$ we get

$$\left(1+\frac{q_{\text{off}}}{q_{\text{on}}}\right)\partial_t a=\left(\frac{q_{\text{off}}}{q_{\text{on}}}+\frac{2\Gamma}{\gamma+2\Gamma}\frac{\frac{\Gamma q_{\text{off}}}{\Gamma+\gamma q_{\text{on}}}\frac{\gamma+2\Gamma}{\Gamma}}{1+\frac{\Gamma q_{\text{off}}}{\Gamma+\gamma q_{\text{on}}}\frac{\gamma+2\Gamma}{\Gamma}}\right)\partial_{xx}a. \tag{S4.64}$$

Now shifting back to dimensional scales and reorganizing terms slightly we obtain

$$\partial_t a=\left(\frac{q_{\text{off}}}{q_{\text{on}}+q_{\text{off}}}\frac{k_BT}{\Gamma}+\frac{q_{\text{on}}}{q_{\text{on}}+q_{\text{off}}}\frac{k_BT}{\Gamma+\frac{1}{2}\left(\frac{k}{q_{\text{off}}}+\frac{q_{\text{on}}}{q_{\text{off}}}\gamma+\gamma\right)}\right)\partial_{xx}a. \tag{S4.65}$$

Using the notations of the main papaer $p_0 = q_{\rm off}/(q_{\rm on}+q_{\rm off})$ the probability to be unbound, $p_1 = 1-p_0$ the probability to have 1 bond and $\gamma_{\rm eff} = \gamma + \frac{k}{q_{\rm off}} + \gamma\frac{q_{\rm on}}{q_{\rm off}}$ we obtain

$$\boxed{\frac{1}{\Gamma_{\rm eff}^{\rm leg+arm}} = \frac{p_0}{\Gamma} + \frac{p_1}{\Gamma + \frac{1}{2}\gamma_{\rm eff}}} \tag{S4.66}$$

that is exactly Eq. (24) in the main paper.

4.3.3 Several arms for 1 leg

Equations set up We consider random attachment and detachment of two springs to one another, in the leg and arm geometry, but now when there are possibly M arms to attach to.

When the springs are unbound the dynamic equations are

$$\begin{cases} \frac{dl}{dt} &= -\frac{k}{\gamma}l + \sqrt{\frac{2k_BT}{\gamma}}\eta(t) \\ \frac{dl_i}{dt} &= -\frac{k}{\gamma}l_i + \sqrt{\frac{2k_BT}{\gamma}}\eta_i(t) \text{ for } i = 1\dots M \\ \frac{dx}{dt} &= \sqrt{\frac{2k_BT}{\Gamma}}\eta_x(t) \end{cases} \tag{S4.67}$$

where l is the length of the top spring, l_i are the lengths of all the bottom springs, and for simplicity here we took $l_0 = 0$.

In the bound state we need to project the dynamics. The dynamic constraint with the bound bottom spring indexed by b is then

$$q(x, l, l_b) = x + l - l_b + l_{\rm bond} = 0 \tag{S4.68}$$

where $l_{\rm bond}$ is the length of the bond, similarly as in the previous section. The constraint process leaves the unbound spring equations completely unaffected and we find after the projection step

$$\begin{cases} \frac{dx}{dt} &= -\frac{k}{2\Gamma+\gamma}(l_1 - l_2) + \sqrt{\frac{8k_BT\Gamma}{(2\Gamma+\gamma)^2}}\eta_x + \sqrt{\frac{2k_BT\gamma}{(2\Gamma+\gamma)^2}}(\eta - \eta_b) \\ \frac{dl}{dt} &= \frac{1}{2}\frac{dx}{dt} - \frac{k}{2\gamma}(l + l_b) + \sqrt{\frac{2k_BT}{4\gamma}}(\eta + \eta_b) \\ \frac{dl_b}{dt} &= -\frac{1}{2}\frac{dx}{dt} - \frac{k}{2\gamma}(l + l_b) + \sqrt{\frac{2k_BT}{4\gamma}}(\eta + \eta_b) \\ \frac{dl_i}{dt} &= -\frac{k}{\gamma}l_i + \sqrt{\frac{2k_BT}{\gamma}}\eta_i(t) \text{ for } i = 1..M \text{ and } i \neq b \end{cases} \tag{S4.69}$$

Generator The generator is similarly

$$\mathcal{L} = \mathcal{Q} + \mathcal{U} = \begin{pmatrix} -Mq_{\rm on} & q_{\rm on} & q_{\rm on} & .. & q_{\rm on} \\ q_{\rm off} & -q_{\rm off} & 0 & ... & 0 \\ q_{\rm off} & 0 & -q_{\rm off} & ... & 0 \\ ... & & & & \\ q_{\rm off} & 0 & 0 & ... & -q_{\rm off} \end{pmatrix} + \mathcal{U} \tag{S4.70}$$

and $\mathcal{U}$ is a diagonal matrix. The first term of $\mathcal{U}$ corresponds to fully unbound dynamics

$$\mathcal{U}_{00} = -\frac{k}{\gamma}l\partial_l + \frac{k_BT}{\gamma}\partial_{ll} + \sum_i\left(-\frac{k}{\gamma}l_i\partial_{l_i} + \frac{k_BT}{\gamma}\partial_{l_il_i}\right) + \frac{k_BT}{\Gamma}\partial_{xx} \tag{S4.71}$$

and further terms correspond each to a bond with the b^{th} arm

$$\begin{aligned} \mathcal{U}_{bb} = &-\frac{k}{2\Gamma+\gamma}(l - l_b)(\partial_x - \frac{1}{2}\partial_{l_b} + \frac{1}{2}\partial_l) - \frac{k}{2\gamma}(l + l_b)(\partial_{l_b} + \partial_l) \\ &+ \frac{2k_BT}{2\Gamma+\gamma}(\partial_x - \frac{1}{2}\partial_{l_b} + \frac{1}{2}\partial_l)^2 + \frac{k_BT}{2\gamma}(\partial_{l_b} + \partial_l)^2 + \sum_{i\neq b}\left(-\frac{k}{\gamma}l_i\partial_{l_i} + \frac{k_BT}{\gamma}\partial_{l_il_i}\right) \end{aligned} \tag{S4.72}$$

With this generator one can check that $\mathcal{L}^\star \pi = 0$ with the natural equilibrium distribution

$$\pi = \frac{1}{Z} \begin{pmatrix} 1 \\ q_{\text{on}}/q_{\text{off}} \\ q_{\text{on}}/q_{\text{off}} \\ ... \end{pmatrix} e^{-kl^2/2k_BT} e^{-\sum_i kl_i^2/2k_BT} \tag{S4.73}$$

where Z is a normalization constant.

Homogenization Taking the usual scalings we get the non-dimensional generator $\mathcal{L} = \frac{1}{\epsilon^2}\mathcal{L}_0 + \frac{1}{\epsilon}\mathcal{L}_1 + \mathcal{L}_2$, where $\mathcal{L}_0 = \mathcal{Q} + \mathcal{U}_0$ where $\mathcal{U}_0$ is diagonal with

$$(\mathcal{U}_0)_{00} = \frac{\Gamma}{\gamma}\left(-l\partial_l + \partial_{ll} + \sum_i (-l_i\partial_{l_i} + \partial_{l_i l_i})\right) \tag{S4.74}$$

$$\begin{aligned}(\mathcal{U}_0)_{bb} = &-\frac{\Gamma}{2(2\Gamma+\gamma)}(l-l_b)(\partial_l - \partial_{l_b}) - \frac{\Gamma}{2\gamma}(l+l_b)(\partial_{l_b} + \partial_l) + \frac{\Gamma}{2(2\Gamma+\gamma)}(\partial_{l_b} - \partial_l)^2 + \frac{\Gamma}{2\gamma}(\partial_{l_b} + \partial_l)^2 \\ &\frac{\Gamma}{\gamma}\sum_{i\neq b}(-l_i\partial_{l_i} + \partial_{l_i l_i})\end{aligned} \tag{S4.75}$$

and $\mathcal{L}_1$ is such that $(\mathcal{L}_1)_{00} = 0$ and

$$(\mathcal{L}_1)_{bb} = -\frac{\Gamma}{2\Gamma+\gamma}(l-l_b)\partial_x + \partial_x(\partial_l - \partial_{l_b})\frac{2\Gamma}{\gamma+2\Gamma} \tag{S4.76}$$

and finally

$$\mathcal{L}_2 = \begin{pmatrix} \partial_{xx} & 0 & 0 & ... \\ 0 & \frac{2\Gamma}{\gamma+2\Gamma}\partial_{xx} & 0 & ... \\ 0 & 0 & \frac{2\Gamma}{\gamma+2\Gamma}\partial_{xx} & ... \end{pmatrix} \tag{S4.77}$$

We now seek an expanded solution f of $\partial_t f = \mathcal{L}f$ as $f = f_0 + \epsilon f_1 + \epsilon^2 f_2 + ...$

At lowest order the resolution gives $f_0 = a(x,t)\begin{pmatrix} 1 \\ 1 \\ 1 \\ ... \end{pmatrix}$, and the associated equilibrium distribution $\pi_0 = \pi$.

At first order we need to solve f_1 and it is useful to seek a genuinely symmetric solution

$$\mathcal{L}_0 f_1 = + \begin{pmatrix} 0 \\ (l-l_1) \\ (l-l_2) \\ ... \end{pmatrix} \frac{\Gamma}{\gamma+2\Gamma}\partial_x a, \text{seeking } f_1 = \begin{pmatrix} u_0 l + u_0' l_1 + u_0' l_2 + .. \\ b_1 l + b_1' l_1 + u_1' l_2 + ... \\ b_1 l + u_1' l_1 + b_1' l_2 + ... \\ ... \end{pmatrix} \partial_x a \tag{S4.78}$$

where u_0, u_0', b_1, b_1' and u_1' are constants. Notice that here u and b refer respectively to unbound and bound contributions, with x and x' corresponding respectively to leg or arm contributions, and the indices

correspond to the number of bonds of the state. The constants obey the system of equations

$$\begin{aligned}
-Mq_{\rm on}u_0 + q_{\rm on}Mb_1 - u_0\frac{\Gamma}{\gamma} &= 0\\
-Mq_{\rm on}u_0' + q_{\rm on}b_1' + (M-1)q_{\rm on}u_1' - u_0'\frac{\Gamma}{\gamma} &= 0\\
q_{\rm off}u_0 - q_{\rm off}b_1 - \frac{\Gamma}{2(2\Gamma+\gamma)}(b_1-b_1') - \frac{b_1+b_1'}{2}\frac{\Gamma}{\gamma} &= \frac{\Gamma}{2\Gamma+\gamma}\\
q_{\rm off}u_0' - q_{\rm off}b_1' + \frac{\Gamma}{2(2\Gamma+\gamma)}(b_1-b_1') - \frac{b_1+b_1'}{2}\frac{\Gamma}{\gamma} &= -\frac{\Gamma}{2\Gamma+\gamma}\\
-q_{\rm off}u_1' + q_{\rm off}u_0' - u_1'\frac{\Gamma}{\gamma} &= 0
\end{aligned} \tag{S4.79}$$

that has a unique solution. For now we do not report the coefficients here for simplicity.

At 2nd order we need to satisfy the Fredholm alternative $\langle \partial_t f_0 - \mathcal{L}_2 f_0 - \mathcal{L}_1 f_1, \pi_0\rangle = 0$. We split up the terms to highlight calculation steps (discarding Z terms to simplify notations, as they would cancel out eventually)

$$\begin{aligned}
\langle \mathcal{L}_1 f_1, \pi_0\rangle =& \sum_i \frac{q_{\rm on}}{q_{\rm off}}\frac{\Gamma}{\gamma+2\Gamma}\langle(-(l-l_i)(b_1 l - b_1' l_i) + 2(b_1-b_1'))\, e^{-l^2/2}e^{-l_i^2/2}\rangle \partial_{xx}a\\
=& M\frac{2\Gamma}{\gamma+2\Gamma}\frac{(b_1-b_1')}{2}\partial_{xx}a
\end{aligned} \tag{S4.80}$$

and

$$\langle \mathcal{L}_2 f_0, \pi_0\rangle = \left(1 + \frac{2\Gamma}{\gamma+2\Gamma}\frac{Mq_{\rm on}}{q_{\rm off}}\right)\partial_{xx}a. \tag{S4.81}$$

Gathering terms as $\langle \partial_t f_0, \pi_0\rangle = \langle \mathcal{L}_2 f_0, \pi\rangle + \langle \mathcal{L}_1 f_1, \pi_0\rangle$ we get

$$\left(1 + M\frac{q_{\rm on}}{q_{\rm off}}\right)\partial_t a = \left(1 + \frac{Mq_{\rm on}}{q_{\rm off}}\frac{2\Gamma}{\gamma+2\Gamma}(1 + \frac{(b_1-b_1')}{2})\right)\partial_{xx}a. \tag{S4.82}$$

Reorganizing terms slightly we arrive at (in dimensional scales)

$$\partial_t a = k_B T\left(\frac{p_{0,M}}{\Gamma} + \frac{p_{1,M}}{\Gamma_{1,M}}\right)\partial_{xx}a. \tag{S4.83}$$

with $p_{0,M} = \frac{q_{\rm off}}{q_{\rm off}+Mq_{\rm on}}$ and $p_{1,M} = 1 - p_{0,M}$ and

$$\Gamma_{1,M} = \frac{\Gamma + \gamma/2}{1 - (b_1 - b_1')/2}. \tag{S4.84}$$

We can further expand $\Gamma_{1,M}$ by using the expressions for b_1 and b_1'. We find

$$\Gamma_{1,M} = \Gamma + \frac{\left(\gamma + \frac{k}{q_{\rm off}}\right)\left(\gamma + \frac{k}{q_{\rm off}} + \gamma\frac{Mq_{\rm on}}{q_{\rm off}}\right)}{\left(\gamma + \frac{k}{q_{\rm off}}\right) + \left(\gamma + \frac{k}{q_{\rm off}} + \gamma\frac{(M-1)q_{\rm on}}{q_{\rm off}}\right)} \tag{S4.85}$$

that is exactly Eq. (25) in the main paper. Notice that, since arm and leg are interchangeable, a similar effect would be observed for a particle with M legs allowed to bind to 1 arm.

Notice that when M is large, we obtain that the above expression simplifies to

$$\Gamma_{1,M} = \Gamma + \gamma_{\rm eff,1,M} \text{ with } \frac{1}{\gamma_{\rm eff,1,M}} = \frac{1}{\gamma_{\rm eff,M,1}} + \frac{1}{\gamma_{\rm eff,1,1}}, \tag{S4.86}$$

with $\gamma_{\rm eff,M,1} = k\left(\frac{1}{q_{\rm off}} + \frac{\gamma}{k}\frac{(M-1)q_{\rm on}+q_{\rm off}}{q_{\rm off}}\right)$ the effective friction due to the leg $\gamma_{\rm eff,1,1} = k\left(\frac{1}{q_{\rm off}} + \frac{\gamma}{k}\right)$ due to arms.

4.3.4 N legs facing M potential arms

2 legs facing 2 arms To understand the dynamics at play in the case of N legs facing M potential arms we first investigate the more specialized 2 for 2 scenario. We number legs as 1 and 2 and arms as 3 and 4. We write the generator for this system directly in the non-dimensional scales. It is a bit lengthy as there are now 7 possible states. We arrange the states as state #1 is the unbound state, states $\#2-5$ correspond to 1 bond states, and states $\#6-7$ to 2 bond states. We write $\mathcal{L}=\mathcal{Q}+\mathcal{U}$. The transition rate matrix for the generator is simply

$$\mathcal{Q}=\frac{1}{\epsilon^2}\begin{pmatrix} -4q_{\text{on}} & q_{\text{on}} & q_{\text{on}} & q_{\text{on}} & q_{\text{on}} & . & . \\ q_{\text{off}} & -q_{\text{off}}-q_{\text{on}} & . & . & . & q_{\text{on}} & . \\ q_{\text{off}} & . & -q_{\text{off}}-q_{\text{on}} & . & . & . & .q_{\text{on}} \\ q_{\text{off}} & . & . & -q_{\text{off}}-q_{\text{on}} & . & .q_{\text{on}} & . \\ q_{\text{off}} & . & . & . & -q_{\text{off}}-q_{\text{on}} & . & .q_{\text{on}} \\ . & q_{\text{off}} & . & q_{\text{off}} & . & -2q_{\text{off}} & . \\ . & . & q_{\text{off}} & . & q_{\text{off}} & . & -2q_{\text{off}} \end{pmatrix} \tag{S4.87}$$

Then we write the diagonal (only non zero) components of $\mathcal{U}$. For the unbound state we have

$$\mathcal{U}_{11}=\frac{1}{\epsilon^2}\frac{\Gamma}{\gamma}\sum_{i=1}^{4}D_{l_i}+\partial_{xx} \tag{S4.88}$$

where $D_{l_i}=-l_i\partial_{l_i}+\partial_{l_il_i}$ is the unbound relaxation operator. Then in the 2..5 states where just one tether is bound we have (for example for the 2 state where tethers say 1 and 3 are bound)

$$\begin{aligned}\mathcal{U}_{22}=&\frac{1}{\epsilon^2}\left(-\frac{\Gamma}{2(2\Gamma+\gamma)}(l_1-l_3)(\partial_{l_1}-\partial_{l_3})-\frac{\Gamma}{2\gamma}(l_1+l_3)(\partial_{l_3}+\partial_{l_1})+\frac{\Gamma}{2(2\Gamma+\gamma)}(\partial_{l_3}-\partial_{l_1})^2+\frac{\Gamma}{2\gamma}(\partial_{l_3}+\partial_{l_1})^2\right)\\&+\frac{1}{\epsilon^2}\frac{\Gamma}{\gamma}\left(D_{l_2}+D_{l_4}\right)+\frac{1}{\epsilon}\frac{\Gamma}{2\Gamma+\gamma}\left(-(l_1-l_3)\partial_x+2\partial_x(\partial_{l_1}-\partial_{l_3})\right)+1\left(\frac{2\Gamma}{2\Gamma+\gamma}\partial_{xx}\right)\end{aligned} \tag{S4.89}$$

and similarly for the other 1 bond states. Finally for the 6 and 7 states, 2 bonds are formed. In these state we have, for example for state #6 that contains the bonds $1-3$ and $2-4$

$$\begin{aligned}\mathcal{U}_{66}=&-\frac{\Gamma}{2\Gamma+2\gamma}(l_1-l_3+l_2-l_4)(\frac{1}{\epsilon}\partial_x-\frac{1}{\epsilon^2}\frac{1}{2}\partial_{l_3}+\frac{1}{\epsilon^2}\frac{1}{2}\partial_{l_1}-\frac{1}{\epsilon^2}\frac{1}{2}\partial_{l_4}+\frac{1}{\epsilon^2}\frac{1}{2}\partial_{l_2})\\&-\frac{1}{\epsilon^2}\frac{\Gamma}{2\gamma}(l_1+l_3)(\partial_{l_3}+\partial_{l_1})-\frac{1}{\epsilon^2}\frac{\Gamma}{2\gamma}(l_2+l_4)(\partial_{l_4}+\partial_{l_2})\\&+\frac{\Gamma}{2(2\Gamma+2\gamma)}\left(2\partial_x+\frac{1}{\epsilon}\left(\partial_{l_1}+\partial_{l_2}-\partial_{l_3}-\partial_{l_4}\right)\right)^2+\frac{\Gamma}{2\gamma}\frac{1}{\epsilon^2}\left[\left(\partial_{l_1}+\partial_{l_3}\right)^2+\left(\partial_{l_2}+\partial_{l_4}\right)^2\right]\end{aligned} \tag{S4.90}$$

and reordering this last expression as a function of the scales in ϵ

$$\begin{aligned}\mathcal{U}_{66}=&\frac{1}{\epsilon^2}\left(-\frac{\Gamma(l_1-l_3+l_2-l_4)}{2(2\Gamma+2\gamma)}(\partial_{l_1}-\partial_{l_3}+\partial_{l_2}-\partial_{l_4})-\frac{(l_1+l_3)\Gamma}{2\gamma}(\partial_{l_3}+\partial_{l_1})-\frac{(l_2+l_4)\Gamma}{2\gamma}(\partial_{l_2}+\partial_{l_4})\right)\\&+\frac{1}{\epsilon^2}\left(\frac{\Gamma}{2(2\Gamma+2\gamma)}\left(\partial_{l_1}+\partial_{l_2}-\partial_{l_3}-\partial_{l_4}\right)^2+\frac{\Gamma}{2\gamma}\left[\left(\partial_{l_1}+\partial_{l_3}\right)^2+\left(\partial_{l_2}+\partial_{l_4}\right)^2\right]\right)\\&+\frac{1}{\epsilon}\left(\frac{2\Gamma}{(2\Gamma+2\gamma)}\partial_x\left(\partial_{l_1}+\partial_{l_2}-\partial_{l_3}-\partial_{l_4}\right)-\frac{\Gamma(l_1-l_3+l_2-l_4)}{2\Gamma+2\gamma}\partial_x\right)\\&+1\left(\frac{2\Gamma}{2\Gamma+2\gamma}\partial_{xx}\right)\end{aligned} \tag{S4.91}$$

Here the equilibrium distribution is

$$\pi = \frac{1}{\sqrt{2\pi}\left(2+4\frac{q_{\rm off}}{q_{\rm on}}+\frac{q_{\rm off}^2}{q_{\rm on}^2}\right)}\left(q_{\rm off}^2/q_{\rm on}^2,\quad q_{\rm off}/q_{\rm on},\quad q_{\rm off}/q_{\rm on},\quad q_{\rm off}/q_{\rm on},\quad q_{\rm off}/q_{\rm on},\quad 1,\quad 1\right)^T. \tag{S4.92}$$

We seek a solution to the expanded generator $\mathcal{L} = \frac{1}{\epsilon^2}\mathcal{L}_0 + \frac{1}{\epsilon}\mathcal{L}_1 + \mathcal{L}_2$ as $f = f_0 + \epsilon f_1 + \epsilon^2 f_2 ....$ No steps change in the resolution compared to previous calculations but for finding the solution at order 1. Here we seek a solution

$$\mathcal{L}_0 f_1 = -\mathcal{L}_1 f_0 = \begin{pmatrix} 0 \\ \frac{1}{2\Gamma+\gamma}(l_1-l_3) \\ \frac{1}{2\Gamma+\gamma}(l_1-l_4) \\ \frac{1}{2\Gamma+\gamma}(l_2-l_4) \\ \frac{1}{2\Gamma+\gamma}(l_2-l_3) \\ \frac{1}{2\Gamma+2\gamma}(l_1-l_3+l_2-l_4) \\ \frac{1}{2\Gamma+2\gamma}(l_1-l_4+l_2-l_3) \end{pmatrix} \Gamma\partial_x a \tag{S4.93}$$

The solution is expected to preserve the symmetries of the problem and therefore we may seek

$$f_1 = \begin{pmatrix} u_0 l_1 + u_0 l_2 + u_0' l_3 + u_0' l_4 \\ b_1 l_1 + u_1 l_2 + b_1' l_3 + u_1' l_4 \\ ... \\ b_2 l_1 + b_2 l_2 + b_2' l_3 + b_2' l_4 \\ ... \end{pmatrix} \partial_x a \tag{S4.94}$$

where b_n, b_n', u_n, u_n' are constants that refer to bound and unbound configurations of the leg or the arms. They solve a linear system of equations that possesses a single solution that we will report below.

The Fredholm alternative at the next order requires $\langle \partial_t f_0 - \mathcal{L}_2 f_0 - \mathcal{L}_1 f_1, \pi\rangle$. We obtain, splitting the relevant contributions

$$\langle \mathcal{L}_1 f_1, \pi\rangle = 0 + \frac{(b_1-b_1')\Gamma}{2\Gamma+\gamma}p_1 + \frac{2(b_2-b_2')\Gamma}{2\Gamma+2\gamma}p_2 \tag{S4.95}$$

and assembling all terms allows to get an effective long time diffusion equation $\partial_t a = \frac{\Gamma}{\Gamma_{\rm eff}^{2,2}}\partial_{xx} a$ where

$$\frac{1}{\Gamma_{\rm eff}^{2,2}} = \frac{1}{\Gamma}p_0 + \frac{1}{\frac{\Gamma+\gamma/2}{\left(1-\frac{b_1-b_1'}{2}\right)}}p_1 + \frac{1}{\frac{\Gamma+2\gamma/2}{\left(1-2\frac{b_2-b_2'}{2}\right)}}p_2 \tag{S4.96}$$

which is similarly as in all cases a weighted harmonic sum of friction coefficients, with p_n the probability to have n bonds.

The system of equations that the constants satisfy is

$$
\begin{aligned}
&-4q_{\rm on}u_0 - u_0 + 2q_{\rm on}b_1 + 2q_{\rm on}u_1 = 0\\
&-4q_{\rm on}u'_0 - u'_0 + 2q_{\rm on}b'_1 + 2q_{\rm on}u'_1 = 0\\
&q_{\rm off}u_0 - q_{\rm off}b_1 - q_{\rm on}b_1 + q_{\rm on}b_2 - \frac{\gamma}{2(2\Gamma+\gamma)}(b_1 - b'_1) - \frac{b_1+b'_1}{2} = \frac{\gamma}{2\Gamma+\gamma}\\
&q_{\rm off}u'_0 - q_{\rm off}b'_1 - q_{\rm on}b'_1 + q_{\rm on}b'_2 + \frac{\gamma}{2(2\Gamma+\gamma)}(b_1 - b'_1) - \frac{b_1+b'_1}{2} = -\frac{\gamma}{2\Gamma+\gamma}\\
&q_{\rm off}u_0 - q_{\rm off}u_1 - q_{\rm on}u_1 + q_{\rm on}b_2 - u_1 = 0\\
&q_{\rm off}u'_0 - q_{\rm off}u'_1 - q_{\rm on}u'_1 + q_{\rm on}b'_2 - u'_1 = 0\\
&q_{\rm off}b_1 + q_{\rm off}u_1 - 2q_{\rm off}b_2 - \frac{2\gamma}{2(2\Gamma+2\gamma)}(b_2 - b'_2) - \frac{b_2+b'_2}{2} = \frac{\gamma}{2\Gamma+2\gamma}\\
&q_{\rm off}b'_1 + q_{\rm off}u'_1 - 2q_{\rm off}b'_2 + \frac{2\gamma}{2(2\Gamma+2\gamma)}(b_2 - b'_2) - \frac{b_2+b'_2}{2} = -\frac{\gamma}{2\Gamma+2\gamma}
\end{aligned}
\tag{S4.97}
$$

Since the bottom and top tethers don't exactly have the same positions it's not possible to simplify further, typically $b_n \neq -b'_n$. This really shows the structure of the equations.

N legs facing M arms The above system of equations allows to generalize the derivation for n bonds in some N legs for M arms structure. For each possible number of bonds say n, the tethers are either unbound (u_n, u'_n) or bound (b_n, b'_n) and can exchange with their counterparts.

When there are n bonds, focusing on a connected pair, one can still bind more pairs, and there are $(M-n)(N-n)$ possible ways to do so. In any case the connected pair will remain connected during that transformation. When there are n bonds, one can unbind n pairs. $n-1$ possibilities lead to the given pair still being bound.

For an unconnected leg (resp. arm), there are only $M-n$ possibilities (resp. $(N-n)$) to form a bond that will connect the unconnected one.

We obtain the general system of equations as

$$
\begin{aligned}
&nq_{\rm off}u_{n-1} - (nq_{\rm off} + (N-n)(M-n)q_{\rm on})u_n + q_{\rm on}(M-n)b_{n+1} + q_{\rm on}(N-n-1)(M-n)u_{n+1} - u_n\frac{\Gamma}{\gamma} = 0\\
&nq_{\rm off}u'_{n-1} - (nq_{\rm off} + (N-n)(M-n)q_{\rm on})u'_n + q_{\rm on}(N-n)b'_{n+1} + q_{\rm on}(M-n-1)(N-n)u'_{n+1} - u'_n\frac{\Gamma}{\gamma} = 0\\
&q_{\rm off}u_{n-1} + (n-1)q_{\rm off}b_{n-1} - (nq_{\rm off} + (N-n)(M-n)q_{\rm on})b_n + q_{\rm on}(N-n)(M-n)b_{n+1}...\\
&\qquad -\frac{n\Gamma}{2(2\Gamma+n\gamma)}(b_n - b'_n) - \frac{b_n+b'_n}{2}\frac{\Gamma}{\gamma} = -\frac{\Gamma}{2\Gamma+n\gamma}\\
&q_{\rm off}u'_{n-1} + (n-1)q_{\rm off}b'_{n-1} - (nq_{\rm off} + (N-n)(M-n)q_{\rm on})b'_n + q_{\rm on}(N-n)(M-n)b'_{n+1}...\\
&\qquad +\frac{n\Gamma}{2(2\Gamma+n\gamma)}(b_n - b'_n) - \frac{b_n+b'_n}{2}\frac{\Gamma}{\gamma} = \frac{\Gamma}{2\Gamma+n\gamma}\\
&\qquad\qquad \frac{\Gamma+n\gamma/2}{1-n(b_n-b'_n)/2} = \Gamma_n
\end{aligned}
\tag{S4.98}
$$

Looking for the average number of bonds contribution, we may assume similarly that for $n = N_b$ we have

$u_n \simeq u_{n-1} \simeq u_n = \bar{u}$, and similarly for other quantities. We thus obtain the closed system of equations

$$\begin{aligned}
-(M-N_b)q_{\rm on}\bar{u} + q_{\rm on}(M-N_b)\bar{b} - \bar{u}\frac{\Gamma}{\gamma} &= 0 \\
-(N-N_b)q_{\rm on}\bar{u}' + q_{\rm on}(N-N_b)\bar{b}' - \bar{u}'\frac{\Gamma}{\gamma} &= 0 \\
q_{\rm off}\bar{u} - q_{\rm off}\bar{b} - \frac{N_b\Gamma}{2(2\Gamma+N_b\gamma)}(\bar{b}-\bar{b}') - \frac{\bar{b}+\bar{b}'}{2}\frac{\Gamma}{\gamma} &= \frac{\Gamma}{2\Gamma+N_b\gamma} \\
q_{\rm off}\bar{u}' - q_{\rm off}\bar{b}' + \frac{N_b\Gamma}{2(2\Gamma+N_b\gamma)}(\bar{b}-\bar{b}') - \frac{\bar{b}+\bar{b}'}{2}\frac{\Gamma}{\gamma} &= -\frac{\Gamma}{2\Gamma+N_b\gamma} \\
\frac{\Gamma+N_b\gamma/2}{1-N_b(\bar{b}-\bar{b}')/2} &= \Gamma_{N_b}
\end{aligned} \tag{S4.99}$$

This finally yields

$$\Gamma_{N_b} = \Gamma + N_b\gamma_{\rm eff,N,M}, \text{ with } \frac{1}{\gamma_{\rm eff,N,M}} = \frac{1}{\gamma_{\rm eff}^{\rm leg}} + \frac{1}{\gamma_{\rm eff}^{\rm arm}}, \tag{S4.100}$$

with the effective friction due to legs as $\gamma_{\rm eff}^{\rm leg} = \gamma + k\left(\frac{1}{q_{\rm off}} + \frac{\gamma}{k}\frac{(M-N_b)q_{\rm on}}{q_{\rm off}}\right)$ and that due to arms $\gamma_{\rm eff}^{\rm arm} = \gamma + k\left(\frac{1}{q_{\rm off}} + \frac{\gamma}{k}\frac{(N-N_b)q_{\rm on}}{q_{\rm off}}\right)$. Here we see that the characteristic binding time (for example for the leg) is $\tau_{\rm on} = 1/(M-N_b)q_{\rm on}$, due to the increased number of possibilities $(M-N_b)$ due to multiple available arms.

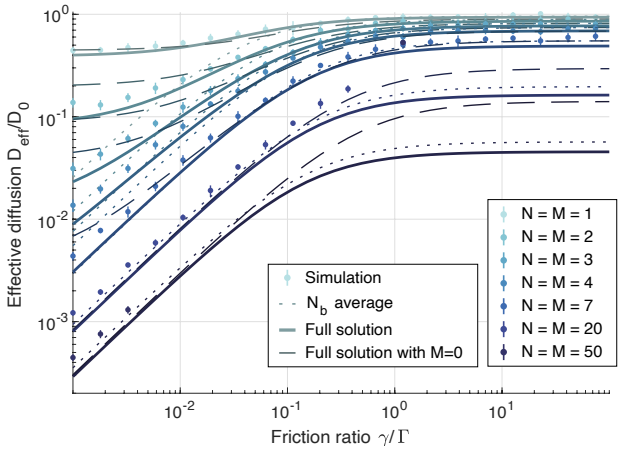

Figure S8: Effective diffusion for systems with an equal number of arms and legs all interacting with one another ($N = M$) from stochastic simulations. We overlay the predictions using Eq. (S4.101) (N_b average) and fully solving for the system of equations Eq. (S4.98) (Full solution). For reference we also show the result of the full system in the case of N legs with $M = 0$ arms, from solving Eq. (S1.20). Here the values of other parameters are $\frac{q_{\rm on}\Gamma}{k} = 1.0$ and $\frac{q_{\rm off}\Gamma}{k} = 0.8$

Here we can explore limiting regimes. If there are as many legs as there are arms we have $M = N$, then the effective friction simplifies to

$$\Gamma_{N_b} = \Gamma + \frac{N_b}{2}\left[\gamma + k\left(\frac{1}{q_{\rm off}} + \frac{\gamma}{k}\frac{(N-N_b)q_{\rm on}}{q_{\rm off}}\right)\right], \tag{S4.101}$$

where we see that the additional friction is divided by 2, as expected from the leg and arm case. One notable difference is that here we see that the characteristic binding time $\tau_{\rm on} = 1/(N-N_b)q_{\rm on}$, due to the increased number of possibilities due to multiple arms and legs. According to the large N limit investigated, $(N-N_b)q_{\rm on}$ does not necessarily diverge. In particular for very sticky systems $(N-N_b) \simeq 0$ and therefore this part does not contribute significantly to the dynamics.

If there are a large number of arms, say $M \gg N_b$, then we find $\gamma_{\text{eff,M,N}} \to \gamma_{\text{eff}}^{\text{arm}}$ is dominated by the arm contributions to the effective friction.

These effective results capture well stochastic simulation results, as shown in Fig. S8.

References

[1] J. P. Lee-Thorp and M. Holmes-Cerfon, "Modeling the relative dynamics of dna-coated colloids," *Soft matter*, vol. 14, no. 40, pp. 8147–8159, 2018.

[2] J. S. Oh, Y. Wang, D. J. Pine, and G.-R. Yi, "High-density peo-b-dna brushes on polymer particles for colloidal superstructures," *Chemistry of Materials*, vol. 27, no. 24, pp. 8337–8344, 2015.

[3] S. Hiki and K. Kataoka, "A facile synthesis of azido-terminated heterobifunctional poly (ethylene glycol) s for "click" conjugation," *Bioconjugate chemistry*, vol. 18, no. 6, pp. 2191–2196, 2007.

[4] Q. Xu, L. Feng, R. Sha, N. Seeman, and P. Chaikin, "Subdiffusion of a sticky particle on a surface," *Physical review letters*, vol. 106, no. 22, p. 228102, 2011.

[5] Y. Wang, Y. Wang, X. Zheng, É. Ducrot, J. S. Yodh, M. Weck, and D. J. Pine, "Crystallization of dna-coated colloids," *Nature communications*, vol. 6, no. 1, pp. 1–8, 2015.

[6] A. Rohatgi, "WebPlotDigitizer: Version 4.5," 2021.

[7] F. Cui, S. Marbach, J. Zheng, M. Holmes-Cerfon, and D. J. Pine, "Comprehensive view of nanoscale interactions between dna-coated colloids," *to appear*, 2021.

[8] S. T. Milner, T. A. Witten, and M. E. Cates, "Theory of the grafted polymer brush," *Macromolecules*, vol. 21, no. 8, pp. 2610–2619, 1988.

[9] P. Varilly, S. Angioletti-Uberti, B. M. Mognetti, and D. Frenkel, "A general theory of dna-mediated and other valence-limited colloidal interactions," *The Journal of chemical physics*, vol. 137, no. 9, p. 094108, 2012.

[10] C. P. Goodrich, M. P. Brenner, and K. Ribbeck, "Enhanced diffusion by binding to the crosslinks of a polymer gel," *Nature communications*, vol. 9, no. 1, pp. 1–8, 2018.

[11] C. Fröhner and F. Noé, "Reversible interacting-particle reaction dynamics," *The Journal of Physical Chemistry B*, vol. 122, no. 49, pp. 11240–11250, 2018.

[12] B. Fogelson and J. P. Keener, "Transport facilitated by rapid binding to elastic tethers," *SIAM Journal on Applied Mathematics*, vol. 79, no. 4, pp. 1405–1422, 2019.

[13] S. Marbach, "Intrinsic fractional noise in nanopores: The effect of reservoirs," *The Journal of Chemical Physics*, vol. 154, no. 17, p. 171101, 2021.

[14] C. Sun, C. Migliorini, and L. L. Munn, "Red blood cells initiate leukocyte rolling in postcapillary expansions: a lattice boltzmann analysis," *Biophysical journal*, vol. 85, no. 1, pp. 208–222, 2003.

[15] G. Pavliotis and A. Stuart, *Multiscale methods: averaging and homogenization*. Springer Science & Business Media, 2008.

[16] A. J. Goldman, R. G. Cox, and H. Brenner, "Slow viscous motion of a sphere parallel to a plane wall—i motion through a quiescent fluid," *Chemical engineering science*, vol. 22, no. 4, pp. 637–651, 1967.

[17] M. Zoli, "End-to-end distance and contour length distribution functions of dna helices," *The Journal of chemical physics*, vol. 148, no. 21, p. 214902, 2018.

[18] J. X. Zhang, J. Z. Fang, W. Duan, L. R. Wu, A. W. Zhang, N. Dalchau, B. Yordanov, R. Petersen, A. Phillips, and D. Y. Zhang, "Predicting dna hybridization kinetics from sequence," *Nature chemistry*, vol. 10, no. 1, pp. 91–98, 2018.

[19] S. Xu, J. Zhan, B. Man, S. Jiang, W. Yue, S. Gao, C. Guo, H. Liu, Z. Li, J. Wang, *et al.*, "Real-time reliable determination of binding kinetics of dna hybridization using a multi-channel graphene biosensor," *Nature communications*, vol. 8, no. 1, pp. 1–10, 2017.

[20] S. Y. Park, A. K. Lytton-Jean, B. Lee, S. Weigand, G. C. Schatz, and C. A. Mirkin, "Dna-programmable nanoparticle crystallization," *Nature*, vol. 451, no. 7178, pp. 553–556, 2008.

[21] S. J. Hurst, A. K. Lytton-Jean, and C. A. Mirkin, "Maximizing dna loading on a range of gold nanoparticle sizes," *Analytical chemistry*, vol. 78, no. 24, pp. 8313–8318, 2006.

[22] H. Ting-Beall, D. Needham, and R. Hochmuth, "Volume and osmotic properties of human neutrophils.," *Blood*, vol. 81, no. 10, pp. 2774–2780, 1993.

[23] S. Chen and T. A. Springer, "Selectin receptor–ligand bonds: Formation limited by shear rate and dissociation governed by the bell model," *Proceedings of the National Academy of Sciences*, vol. 98, no. 3, pp. 950–955, 2001.

[24] J.-Y. Shao, H. P. Ting-Beall, and R. M. Hochmuth, "Static and dynamic lengths of neutrophil microvilli," *Proceedings of the National Academy of Sciences*, vol. 95, no. 12, pp. 6797–6802, 1998.

[25] J. Fritz, A. G. Katopodis, F. Kolbinger, and D. Anselmetti, "Force-mediated kinetics of single p-selectin/ligand complexes observed by atomic force microscopy," *Proceedings of the National Academy of Sciences*, vol. 95, no. 21, pp. 12283–12288, 1998.

[26] U. S. Schwarz and R. Alon, "L-selectin-mediated leukocyte tethering in shear flow is controlled by multiple contacts and cytoskeletal anchorage facilitating fast rebinding events," *Proceedings of the National Academy of Sciences*, vol. 101, no. 18, pp. 6940–6945, 2004.

[27] R. Alon, D. A. Hammer, and T. A. Springer, "Lifetime of the p-selectin-carbohydrate bond and its response to tensile force in hydrodynamic flow," *Nature*, vol. 374, no. 6522, pp. 539–542, 1995.

[28] R. Alon, S. Chen, K. D. Puri, E. B. Finger, and T. A. Springer, "The kinetics of l-selectin tethers and the mechanics of selectin-mediated rolling," *The Journal of cell biology*, vol. 138, no. 5, pp. 1169–1180, 1997.

[29] C. Korn and U. Schwarz, "Dynamic states of cells adhering in shear flow: from slipping to rolling," *Physical review E*, vol. 77, no. 4, p. 041904, 2008.

[30] P. Mehta, R. D. Cummings, and R. P. McEver, "Affinity and kinetic analysis of p-selectin binding to p-selectin glycoprotein ligand-1," *Journal of Biological Chemistry*, vol. 273, no. 49, pp. 32506–32513, 1998.

[31] O. Dwir, A. Solomon, S. Mangan, G. S. Kansas, U. S. Schwarz, and R. Alon, "Avidity enhancement of l-selectin bonds by flow: shear-promoted rotation of leukocytes turn labile bonds into functional tethers," *The Journal of cell biology*, vol. 163, no. 3, pp. 649–659, 2003.

[32] S. Bakshi, A. Siryaporn, M. Goulian, and J. C. Weisshaar, "Superresolution imaging of ribosomes and rna polymerase in live escherichia coli cells," *Molecular microbiology*, vol. 85, no. 1, pp. 21–38, 2012.

[33] E. Miller, T. Garcia, S. Hultgren, and A. F. Oberhauser, "The mechanical properties of e. coli type 1 pili measured by atomic force microscopy techniques," *Biophysical journal*, vol. 91, no. 10, pp. 3848–3856, 2006.

[34] O. Yakovenko, V. Tchesnokova, E. V. Sokurenko, and W. E. Thomas, "Inactive conformation enhances binding function in physiological conditions," *Proceedings of the National Academy of Sciences*, vol. 112, no. 32, pp. 9884–9889, 2015.

[35] M. M. Sauer, R. P. Jakob, T. Luber, F. Canonica, G. Navarra, B. Ernst, C. Unverzagt, T. Maier, and R. Glockshuber, "Binding of the bacterial adhesin fimh to its natural, multivalent high-mannose type glycan targets," *Journal of the American Chemical Society*, vol. 141, no. 2, pp. 936–944, 2018.

[36] M. M. Sauer, R. P. Jakob, J. Eras, S. Baday, D. Eriş, G. Navarra, S. Berneche, B. Ernst, T. Maier, and R. Glockshuber, "Catch-bond mechanism of the bacterial adhesin fimh," *Nature communications*, vol. 7, no. 1, pp. 1–13, 2016.

[37] F. C. Neidhardt, J. L. Ingraham, and M. Schaechter, *Physiology of the bacterial cell; a molecular approach*. No. 589.901 N397, Sinauer associates, 1990.

[38] C. B. Korn, S. Klumpp, R. Lipowsky, and U. S. Schwarz, "Stochastic simulations of cargo transport by processive molecular motors," *The Journal of chemical physics*, vol. 131, no. 24, p. 12B624, 2009.

[39] F. Gibbons, J.-F. Chauwin, M. Despósito, and J. V. José, "A dynamical model of kinesin-microtubule motility assays," *Biophysical journal*, vol. 80, no. 6, pp. 2515–2526, 2001.

[40] T. Duke and S. Leibler, "Motor protein mechanics: a stochastic model with minimal mechanochemical coupling," *Biophysical journal*, vol. 71, no. 3, pp. 1235–1247, 1996.

[41] R. D. Vale, T. Funatsu, D. W. Pierce, L. Romberg, Y. Harada, and T. Yanagida, "Direct observation of single kinesin molecules moving along microtubules," *Nature*, vol. 380, no. 6573, pp. 451–453, 1996.

[42] C. Leduc, O. Campàs, K. B. Zeldovich, A. Roux, P. Jolimaitre, L. Bourel-Bonnet, B. Goud, J.-F. Joanny, P. Bassereau, and J. Prost, "Cooperative extraction of membrane nanotubes by molecular motors," *Proceedings of the National Academy of Sciences*, vol. 101, no. 49, pp. 17096–17101, 2004.

[43] J. Wu, A. H. Corbett, and K. M. Berland, "The intracellular mobility of nuclear import receptors and nls cargoes," *Biophysical journal*, vol. 96, no. 9, pp. 3840–3849, 2009.

[44] I. V. Aramburu and E. A. Lemke, "Floppy but not sloppy: Interaction mechanism of fg-nucleoporins and nuclear transport receptors," in *Seminars in cell & developmental biology*, vol. 68, pp. 34–41, Elsevier, 2017.

[45] R. Y. Lim, N.-P. Huang, J. Köser, J. Deng, K. A. Lau, K. Schwarz-Herion, B. Fahrenkrog, and U. Aebi, "Flexible phenylalanine-glycine nucleoporins as entropic barriers to nucleocytoplasmic transport," *Proceedings of the National Academy of Sciences*, vol. 103, no. 25, pp. 9512–9517, 2006.

[46] L.-C. Tu, G. Fu, A. Zilman, and S. M. Musser, "Large cargo transport by nuclear pores: implications for the spatial organization of fg-nucleoporins," *The EMBO journal*, vol. 32, no. 24, pp. 3220–3230, 2013.

[47] A. Harris, G. Cardone, D. C. Winkler, J. B. Heymann, M. Brecher, J. M. White, and A. C. Steven, "Influenza virus pleiomorphy characterized by cryoelectron tomography," *Proceedings of the National Academy of Sciences*, vol. 103, no. 50, pp. 19123–19127, 2006.

[48] V. Reiter-Scherer, J. L. Cuellar-Camacho, S. Bhatia, R. Haag, A. Herrmann, D. Lauster, and J. P. Rabe, "Force spectroscopy shows dynamic binding of influenza hemagglutinin and neuraminidase to sialic acid," *Biophysical journal*, vol. 116, no. 6, pp. 1037–1048, 2019.

[49] C. Sieben, C. Kappel, R. Zhu, A. Wozniak, C. Rankl, P. Hinterdorfer, H. Grubmüller, and A. Herrmann, "Influenza virus binds its host cell using multiple dynamic interactions," *Proceedings of the National Academy of Sciences*, vol. 109, no. 34, pp. 13626–13631, 2012.

[50] N. K. Sauter, M. D. Bednarski, B. A. Wurzburg, J. E. Hanson, G. M. Whitesides, J. J. Skehel, and D. C. Wiley, "Hemagglutinins from two influenza virus variants bind to sialic acid derivatives with millimolar dissociation constants: a 500-mhz proton nuclear magnetic resonance study," *Biochemistry*, vol. 28, no. 21, pp. 8388–8396, 1989.

[51] M. Müller, D. Lauster, H. H. Wildenauer, A. Herrmann, and S. Block, "Mobility-based quantification of multivalent virus-receptor interactions: New insights into influenza a virus binding mode," *Nano letters*, vol. 19, no. 3, pp. 1875–1882, 2019.

[52] T. Sakai, S. I. Nishimura, T. Naito, and M. Saito, "Influenza a virus hemagglutinin and neuraminidase act as novel motile machinery," *Scientific reports*, vol. 7, no. 1, pp. 1–11, 2017.

[53] M. Laue, A. Kauter, T. Hoffmann, L. Möller, J. Michel, and A. Nitsche, "Morphometry of sars-cov and sars-cov-2 particles in ultrathin plastic sections of infected vero cell cultures," *Scientific reports*, vol. 11, no. 1, pp. 1–11, 2021.

[54] J. Yang, S. J. Petitjean, M. Koehler, Q. Zhang, A. C. Dumitru, W. Chen, S. Derclaye, S. P. Vincent, P. Soumillion, and D. Alsteens, "Molecular interaction and inhibition of sars-cov-2 binding to the ace2 receptor," *Nature communications*, vol. 11, no. 1, pp. 1–10, 2020.

[55] W. Cao, C. Dong, S. Kim, D. Hou, W. Tai, L. Du, W. Im, and X. F. Zhang, "Biomechanical characterization of sars-cov-2 spike rbd and human ace2 protein-protein interaction," *Biophysical journal*, vol. 120, no. 6, pp. 1011–1019, 2021.

[56] M. Ponga, "Quantifying the adhesive strength between the sars-cov-2 s-proteins and human receptor and its effect in therapeutics," *Scientific reports*, vol. 10, no. 1, pp. 1–7, 2020.

[57] A. C. Walls, Y.-J. Park, M. A. Tortorici, A. Wall, A. T. McGuire, and D. Veesler, "Structure, function, and antigenicity of the sars-cov-2 spike glycoprotein," *Cell*, vol. 181, no. 2, pp. 281–292, 2020.

[58] S. Marbach and M. Holmes-Cerfon, "Can mass change the diffusion coefficient of dna-coated colloids?," *arXiv preprint arXiv:2112.05266*, 2021.

[59] B. Fogelson and J. P. Keener, "Enhanced nucleocytoplasmic transport due to competition for elastic binding sites," *Biophysical journal*, vol. 115, no. 1, pp. 108–116, 2018.

[60] P. K. Jana and B. M. Mognetti, "Translational and rotational dynamics of colloidal particles interacting through reacting linkers," *Physical Review E*, vol. 100, no. 6, p. 060601, 2019.